澳門大學
UNIVERSIDADE DE MACAU
UNIVERSITY OF MACAU

Outstanding Academic Papers by Students
學生優秀作品

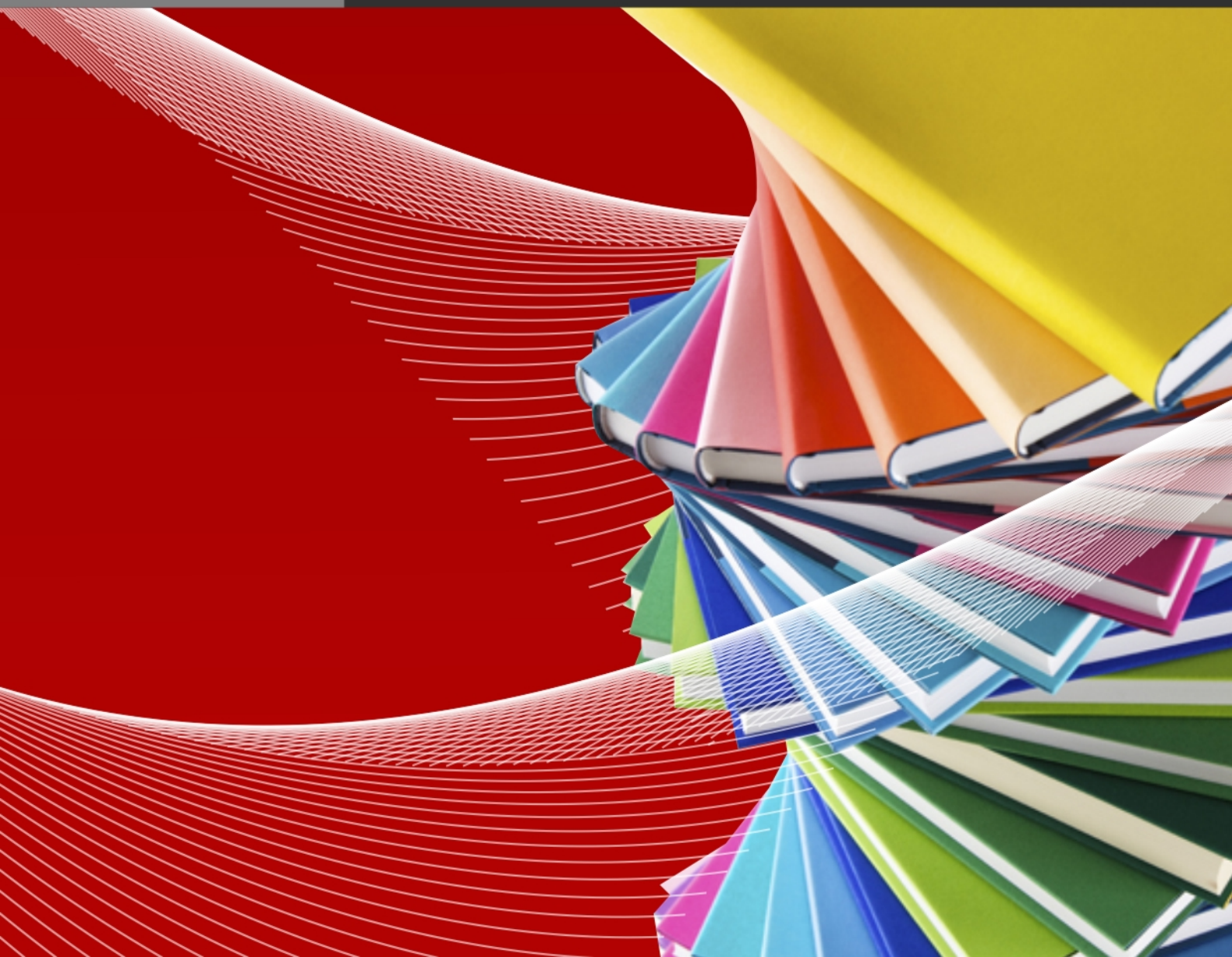

Design of a Two-Axis Micro-Motion Machine for Precision Alignment

by

Law Man Kit (D-B1-2766-4)

Chiang Ka Cheong (D-B1-2775-1)

B.Sc. in Electromechanical Engineering

2014/2015

Faculty of Science and Technology
University of Macau

Design of a Two-Axis Micro-Motion Machine for Precision Alignment

by

Law Man Kit (D-B1-2766-4)

Chiang Ka Cheong (D-B1-2775-1)

Final Year Project Report submitted in partial fulfillment of the requirements for the degree of

B.Sc. in Electromechanical Engineering

Faculty of Science and Technology

University of Macau

2014/2015

University of Macau

Abstract

Design of a Two-Axis Micro-Motion Machine for Precision Alignment

by

Law Man Kit (D-B1-2766-4)

Chiang Ka Cheong (D-B1-2775-1)

Project Supervisor: Dr. Xu Qingsong

In this report, the design procedure of a two-axis micro motion machine prototype is proposed. Not only the fabrication, parts machining and assembly processes, but also the experimental measurement setup, the data collection and analysis procedures are presented clearly. The goals of this project are:

(1) The design provide precision alignment ability;

(2) Each axis for the prototype provides a long alignment distance range of ±5mm;

(3) Well-decoupling motion in the two axes.

The design is devised base on the metal flexure mechanism and the structure is named multi-stage leaf springs, which allow a precise moving without friction. Two voice coil motors are used to drive the two-axis motion, respectively. The flexure mechanism design is validated through finite-element analysis (FEA) simulation study. And the results confirm that the mechanism can provide over ±7mm without any failure in each axis, which verifies that the design is favorable. Besides, a series of experimental studies are

performed on the prototype by using LabVIEW software. Experimented results show that the designed performance of the machine is close to the goal.

Table of Contents

LIST OF FIGURES

Number *Page*

LIST OF TABLES

Number *Page*

LIST OF ABBREVIATIONS

CAD	Computer-Aided Design
FEM	Finite Element Analysis
MCPF	Multi-stage Compound Parallelogram Flexure
PC	Personal Computer
VCM	Voice Coil Motor
DAC	Digital-to-analog converter
ADC	Analog-to-digital converter

ACKNOWLEDGMENTS

Firstly, the authors wish to express their deep gratitude to their project supervisor, Dr. Xu Qingsong, who guides the authors to take a basic concept for the design, schemes the goals that are required to achieve in every short-term and help them to realize the design into a prototype. Besides, he gives the serious advices and suggestion after every progress reporting, even some confusing question are asked, he listens to the authors carefully, simplifies those question and explain to them patiently. As the result of it, they have gained lots of knowledge from Dr. Xu related to the project design.

Furthermore, the authors also like to express their thankfulness to Dr. L.M. Tam, Dr. H.K. Tam, for providing the friendly working environment; Mr. S.O. Shum, Mr. H.S. Chio, Mr. F. T. Cheang, Mr. C. F. Kwok, Mr. S.C. Wan for providing the friendly parts machining, technical support and design suggestion.

CHAPTER 1: INTRODUCTION

Nowadays, there are many precision instruments that are able to provide high accuracy. Their typical applications include scanning probe microscopy (SPM), imaging [1], IC assembly, metrology, nanolithography and micromanipulation [2], etc. The quality of these technologies and the applications area are increasing continuously. The technique developments of micro/nano-positioning are acting as an important character in the precision engineering [3-8]. Therefore, in order to achieve a high accuracy, the micro-motion machine must be applied, especially in the field of microscopy. However, the limitation of the moving range of scanning and working place has obstructed the creation process. As far as the kinematic schemes of the parts are concerned, the problems of achieving the compliant and long range motion need to be addressed.

For overcoming the aforementioned challenge in the precision alignment work, a compliant and flexure-based mechanism can be employed. Most of the metal alloy materials can provide a good elasticity and can be designed to produce a flexure mechanism, and is able to form a deformation phenomenon to reach the high range movement and displacement. Hence, the problems of the friction and the backlash can be eliminated simultaneously. In the literature, several kinds of flexure mechanisms had been designed and applied in the nanotechnology research area [9-12]. For those nano-positioners, the motion quality, precision and accuracy of the design should be concerned in the most priority position, so do our project. By applying the flexure mechanism, even it can overcome the friction and weakness, the selection of the

material used in the prototype is the most important part. The material should not be broken in the alignment procedure. As the result of it, Aluminum 7075-T6 is the most suitable material for the stage body. This material can provide a high strength and light in weight, far better than other type of aluminum alloys. Furthermore, to achieve a desired displacement, the VCM (voice coil motor) and a serial of instrument are used, so that the VCM can drive the flexure structural to form the micro-movement, and the result can be recorded and shown at the same time. [13-14]

In this project, the designed machine should be able to present the alignment in two-axis. But there is one challenge for the two-axis mechanism design – decoupling. If there are two or more systems or movements take the kinematics effects to each other by the interaction, it should isolate or separate the influence force and kinematics properties for each moving axis motion in a mathematics calculation. In this project, the presented design realizes the decoupling by devising a new mechanical structure. The standard of our goal in decoupling is that the displacement of one parasitic axis should not be more than 1% of the main axis motion. For example, when one of the main axis movement is recorded 5 mm, then the other parasitic axis movement should not exceed 0.05 mm.

The CAD model of the design prototype is shown in Fig. 1. The two axes for the alignment are X-axis and Z-axis. The main contribution of the design is that the prototype can provide a movable precision alignment stage of microscope to give the adjustment, and also facilitate the auto-focusing imaging work.

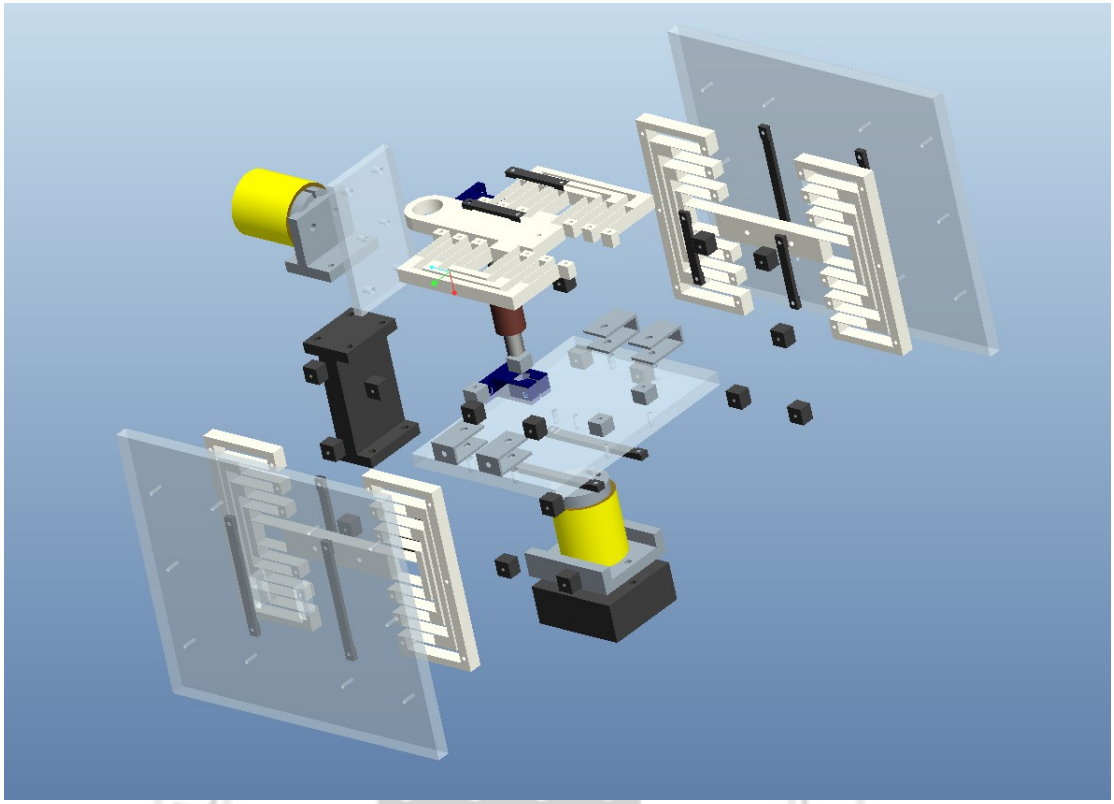

Fig 1. 1 The explosion view for the design

CHAPTER 2: MECHANISM DESIGN

2.1 Flexure Structure Analysis and Selection

For the purpose of alignment with two-axis, the designed mechanism should be able to move in two axial directions. For the design, the desired displacement is ±5mm, total in 10mm, which can achieve the position to the target point in two directions and provide no influence force to each other.

Firstly, the basic structural of the flexure mechanism should be decided. In the literature, two known types of flexures are popular to achieve. They are elliptic hinge structure (see Fig. 2.1) and the beam element (see Fig. 2.2).

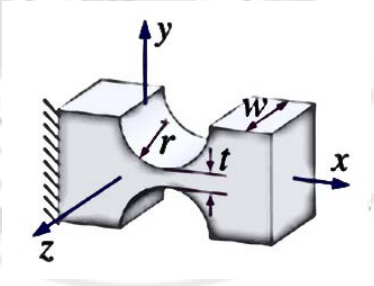

Fig 2. 1 Elliptic (circle) hinge

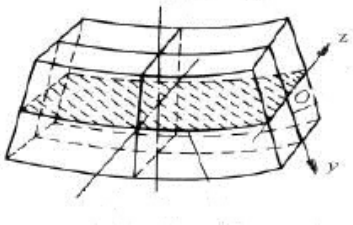

Fig 2. 2 Beam element [20]

2.1.1 Elliptic Hinge

For the elliptic hinge, the deformation will process at the central of the hinge. The major parameter (a, b and t) of an elliptic hinge are shown in Fig.2.3, a parameter d represents the thickness of the elliptic hinge, which is not shown.

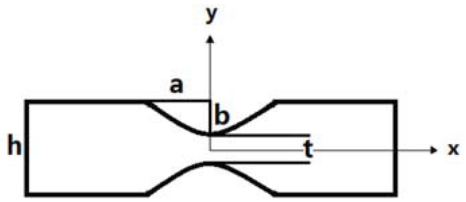

Fig 2. 3 The major parameters of elliptic hinge

The curve function in the central of the hinge is obtained and can be expressed as [16]:

$$y(x) = b + \frac{t}{2} - b\left(1 - \frac{x^2}{a^2}\right)^{0.5} \quad (1)$$

The rotational angle and rotational stiffness of the elliptic (circle) hinge are shown below [17]:

$$\theta = \frac{3M}{2Ed}\int_x \frac{1}{y(x)^3}dx \quad (2)$$

$$k_a = \frac{3Edl}{2}\int_x \frac{1}{x(y)^3}dx \quad (3)$$

Assume that the design force is applied at the edge of the hinge in the y direction. The main function to get the displacement in the y direction is [12]:

$$\Delta_y = \frac{F_y}{2ED}\int_x \frac{1}{y(x)}dx \quad (4)$$

Combining the previous equations and expressing the integral, the displacement function in the y direction can be reached as [18]:

$$\Delta_y = \frac{3F_y a^2}{2EDb^2}\left\{\left[\frac{1}{2\left(1+\frac{t}{2b}\right)} + \frac{1-\left(\frac{t}{2b}\right)}{2\left(\frac{t}{2b}\right)} - 0.5\left[\frac{1+4\frac{t}{2b}+2\left(\frac{t}{2b}\right)^2}{\left(1+\frac{t}{2b}\right)\left[\left(\frac{t}{2b}\right)^2+\frac{t}{2b}\right]}\right] + \left(\frac{4\left(1+\frac{t}{2b}\right)}{\sqrt{\left[\left(\frac{t}{2b}\right)^2+\frac{t}{2b}\right]}} - \frac{2\left(1+\frac{t}{2b}\right)}{\left(2\left(\frac{t}{2b}\right)^2+\frac{t}{2b}\right)^{1.5}}\right)\times \left(arctan\left(\sqrt{\frac{2+\frac{t}{2b}}{\frac{t}{2b}}}\right) - 180\right)\right]\right\} \quad (5)$$

By observing the expression, the parameter of the elliptic hinge is proportional to the displacement in the y direction. However, the desired size of the prototype is small in size. Using the elliptic (circle) hinge, the prototype should be machined in a quite large in size aims to reach 10mm displacement. It is difficult to assemble and not practical.

2.1.2 The Leaf Flexure

The leaf flexure is the positioning structure based on the application of beam element. For the beam element, the original central axis will offset a displacement which is shown in Fig 2.4.To accomplish a wide motion range and solve the central offset problem, leaf flexure is usually employed [18].

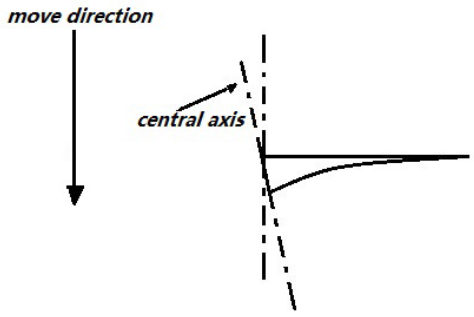

Fig 2. 4 The central axis offset of a beam element [18]

The central axis should be keep in the F direction, in a particular direction perpendicular to the element, the movement should be combined with another beam

deformation, which are shown in Fig 2.5 and Fig 2.6.Thus, the combination structural is shown in Fig 2.7. [18]

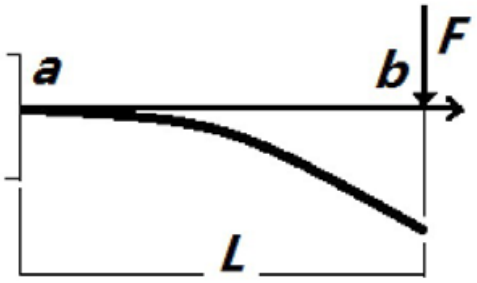

Fig 2. 5 Beam deformation due to force

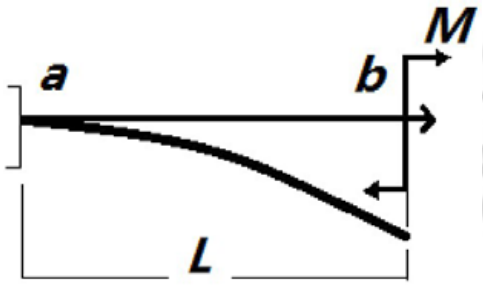

Fig 2. 6 Beam deformation due to moment

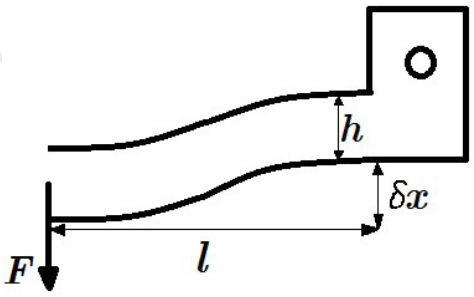

Fig 2. 7 The combination deformation of beam element.

Due to the combination deformation, the rotation angels at the two ends of the element are equal to each other. Therefore, the displacement equation can be easily gotten,

$$\delta_x = \frac{Fl^2}{2EI} - \frac{Ml}{EI} \tag{6}$$

$$0 = \frac{Fl^3}{2EI} - \frac{Ml^2}{EI} \tag{7}$$

Solving (6) and (7), yields

$$F=\frac{2M}{l} \tag{8}$$

$$\delta_x = \frac{Fl^3}{12EI} \tag{9}$$

Because of the deformation is bi-directional. Hence, the total displacement is

$$\Delta_x = 2\delta_x = \frac{\frac{2M}{l}\times 2l^3}{12EI} \tag{10}$$

For the moment M, it can be calculated from the stress formula:

$$I = (bh^3)/12 \tag{11}$$

$$\sigma_{max} = (M_{max}y) \times I_z = (M_{max}\frac{h}{2}) \times I_z \tag{12}$$

$$M_{max} = \frac{\sigma_{max}bh^2}{6} \tag{13}$$

By substituting (13) and (11) into (10)

$$\Delta x_{max} = \frac{F}{K} = 2N\sigma_{max}l^2/3hE \tag{14}$$

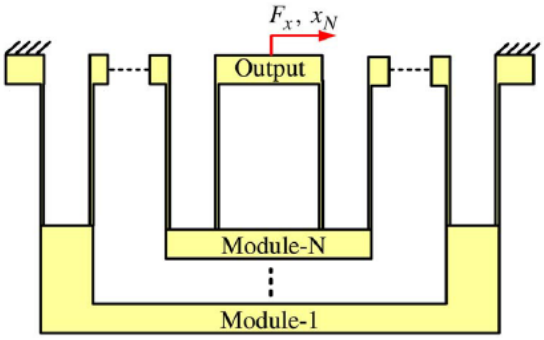

Fig 2. 8 The combination deformation of beam element [3]

For the result, the leaf spring can provide a larger displacement with small parameter. In the literature, an idea of multi-stage compound parallelogram flexure (MCPF) is proposed [19], as shown in Fig 2.8, and the development of this concept is based on the beam element model in the previous combination, which reaches the most compact structure and stable stage design. As the result of it, the compact structure of the leaf flexures associated with the MCPF has been selected to form the moving stage.

2.2 PROCEDURE OF THE DECOUPLING SOLVING, SHAPE DESIGN OF MCPF AND CAD MODEL PROCESS

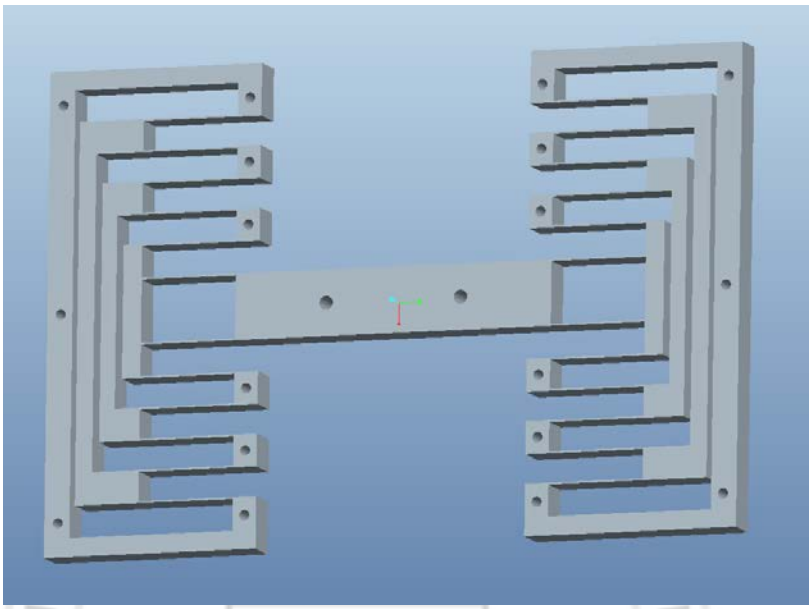

Fig 2. 9 The CAD model for the Z-axis multi-leaf compound structure

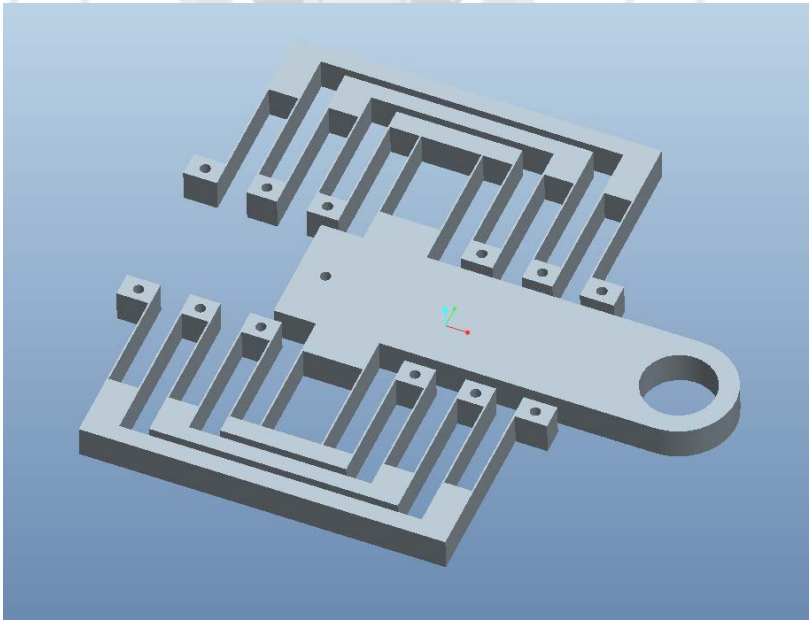

Fig 2. 10 The CAD model for the X-axis multi-leaf compound structure

After a series of structure analysis and calculation, the final structure is selected. The CAD model of the X-axis and Z-axis mechanism are designed independently, which are shown in Fig 2.9 and Fig 2.10. However, the most serious objective in this project is the solution of decoupling, which means to isolate the actuators of 2-axis motion. To achieve a decoupled motion, two platforms should able to give the displacement simultaneously. In the literature, a monolithic parallel kinematics 2-axis stage has been created and is qualified to provide a well-decoupled and large precision range design [9]. The design is a compact multi-stages structure and each of the stage can provide a large tolerating ability against the other axial force. Here, a new structure design is desired, which can also give the isolation ability to provide a well-decoupled precision.

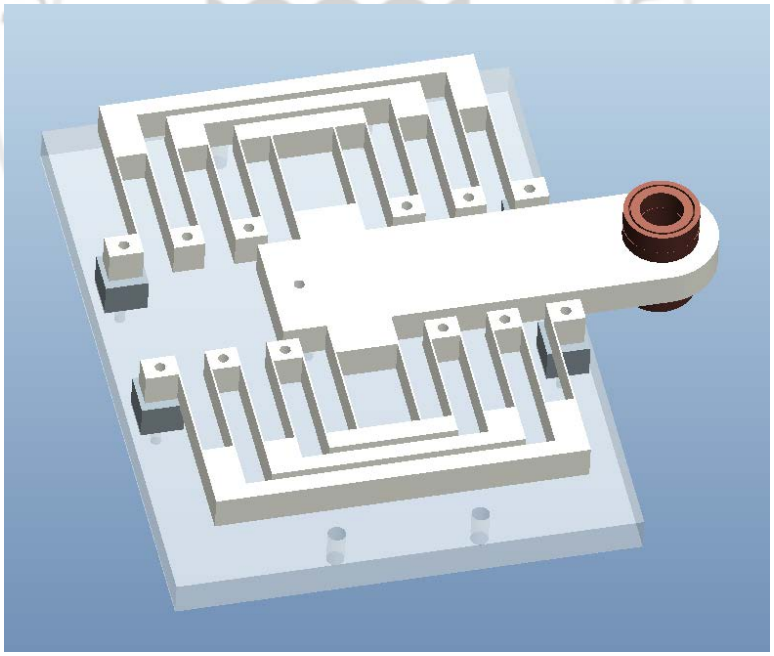

Fig 2. 11 The X-axis stucture is installed with a linear bearing on the platform

In Fig 2.11, a linear bearing is installed at the end of the X-axis structure and is supported by a platform. The reason to install a linear bearing with the X-axis structure is to give a limitation in the moving direction. Four supports are installed below the structure to rise it up. An optical rod is fixed with two holders and passes through the bearing to form a standard linear orienting unit. The two holders are located and fixed on a board and are perpendicular to each other. As Fig 2.12 shows, the VCM is connected to the board and is able to provide the X-direction force. Thus, whatever the position of the X-axis platform located on the optical rod, the VCM can fully transmit and provide the driving force to the X-axis structure, as shown in Fig 2.13.

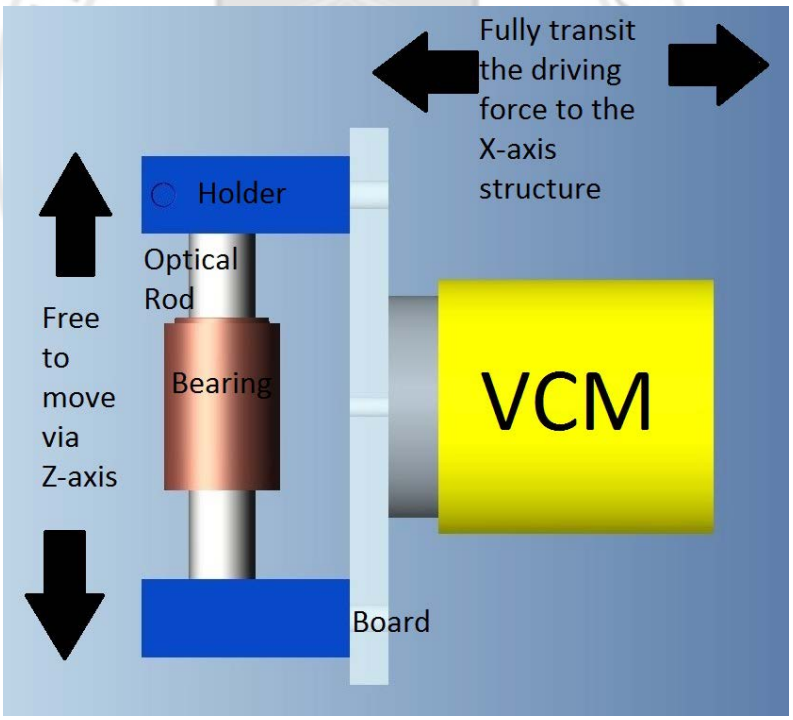

Fig 2. 12 The 2 holders hold the optical rod that pass through the linear bearing to form a linear oriented unit and is able to let the VCD to transit the axial force to the X-axis structure.

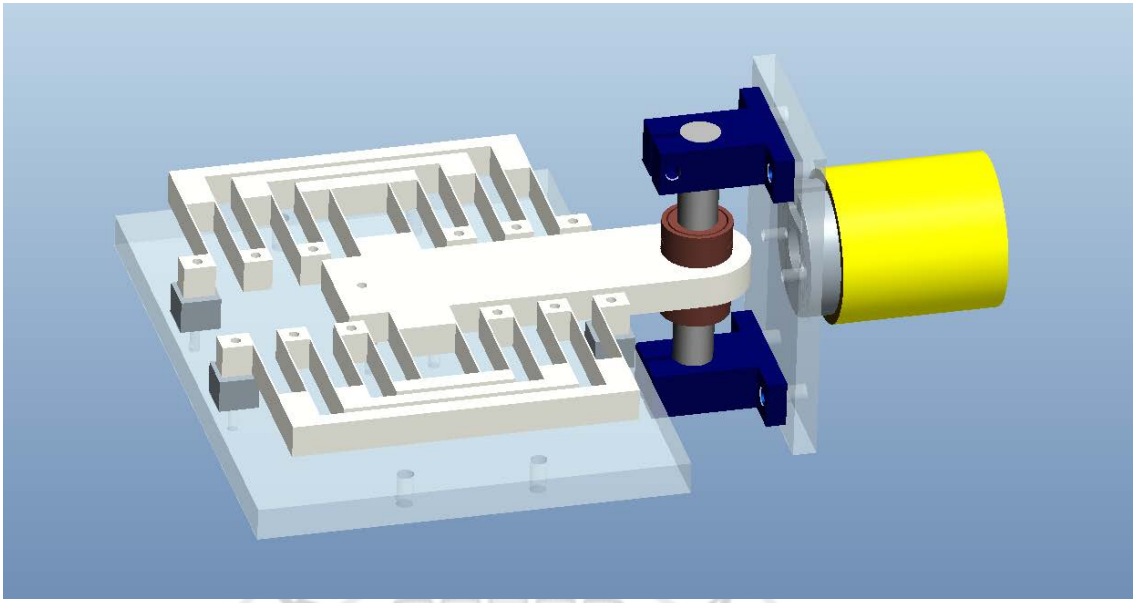

Fig 2. 13 The orientation view of the installation for X-axis platform

Finally, another VCM is installed under the aforementioned platform to provide the Z-axis force. There are 2 Z-axis structures in total and each of them is installed with 2 U-shaped supporters (as shown in Fig. 2.14). It aims to support and carry the X-axis platform and provide the Z-axis precision alignment function simultaneously (as shown in Figs. 2.15 and 2.16).

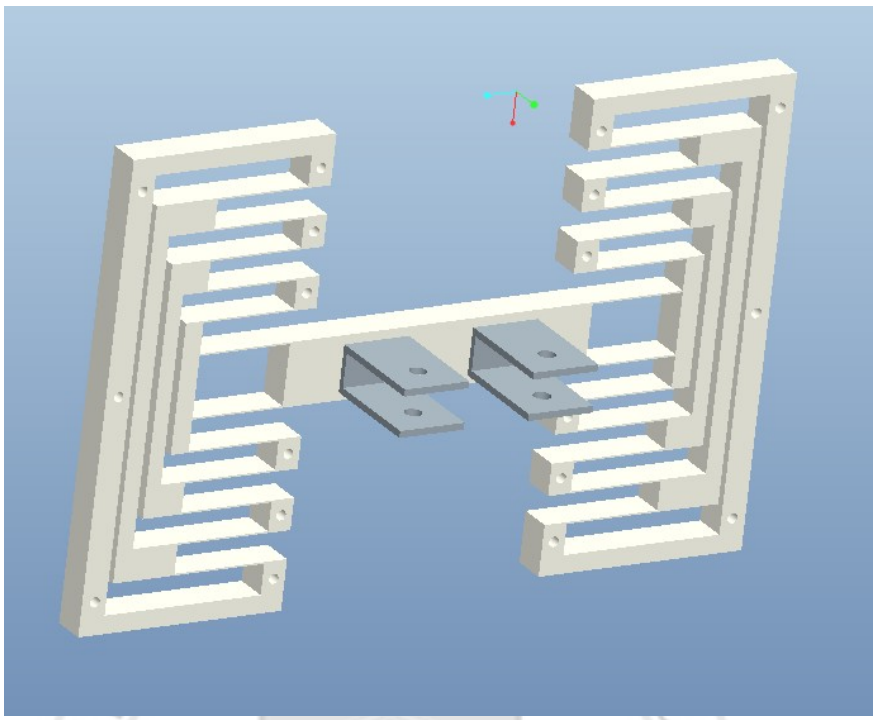

Fig 2. 14 Z-axis structures are installed with 2 U-shaped supporters

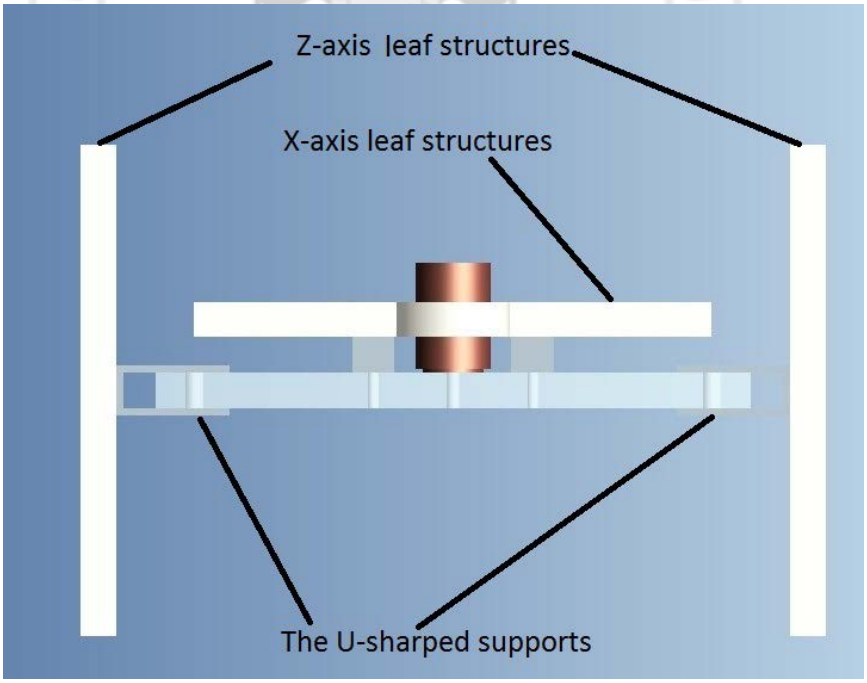

Fig 2. 15 The side view of the assembly model of the X-axis and Z-axis structures

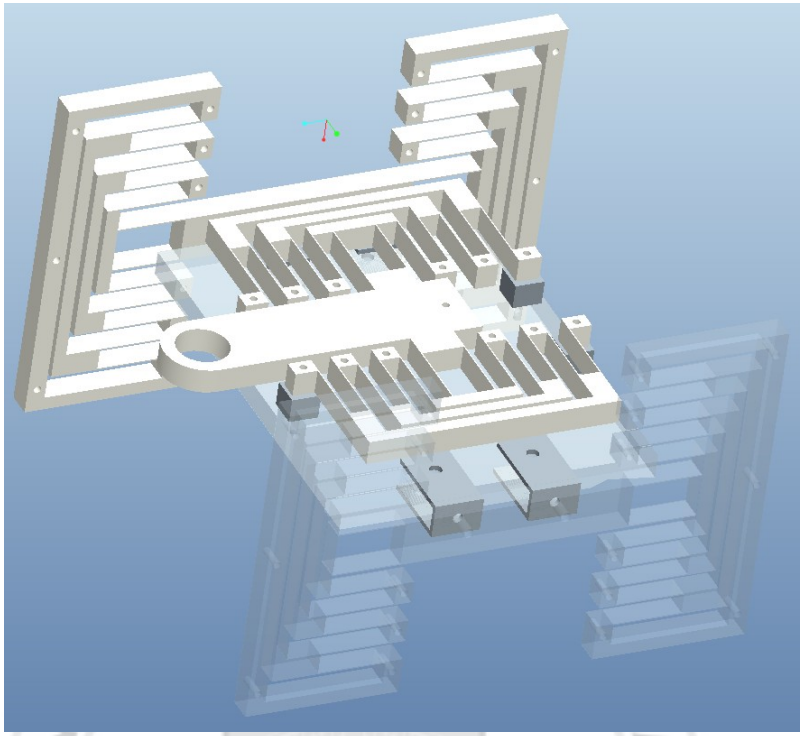

Fig 2. 16 the orientation view of the combined installation of X-axis and Z-axis

By a series of prediction and simulation, the prototype rudiment design is decided. The decoupling solution is based on applying the mechanical motion theory; one structure carries the other one, so that they are able to move independently.

Moreover, in order to make sure that the prototype is absolutely vertical to the ground, 3 Acrylic sheet boards are installed at the back and down positions. The reason for selecting the acrylic sheet for the basement material of the prototype is that it has a series of the advantages: low weight (density=1.19 g/cm^3), cheap price and easy to machine into desire dimension and shape. Also, the acrylic sheet has a high impact resistance that would be the best choice for the design. Furthermore, two supporters made by aluminum are designed and machined to a particular size for each VCM.

Afterwards, for more stable performance of the structure, four “bridges” are designed in a particular dimension for one leaf-structure, aiming to provide the consistency between the leaves. Totally, 12 bridges are designed. Finally, the CAD overview of the design model of the 2-axis precision alignment machine is shown in Fig 2.17 after all the parts and structures are assembled.

In addition, a schematic diagram of the designed machine is shown in Fig 2.18. It is observed that the structure is a 2-PP (P stands for prismatic joint) parallel mechanism. It is able to provide a motion decoupling in theory.

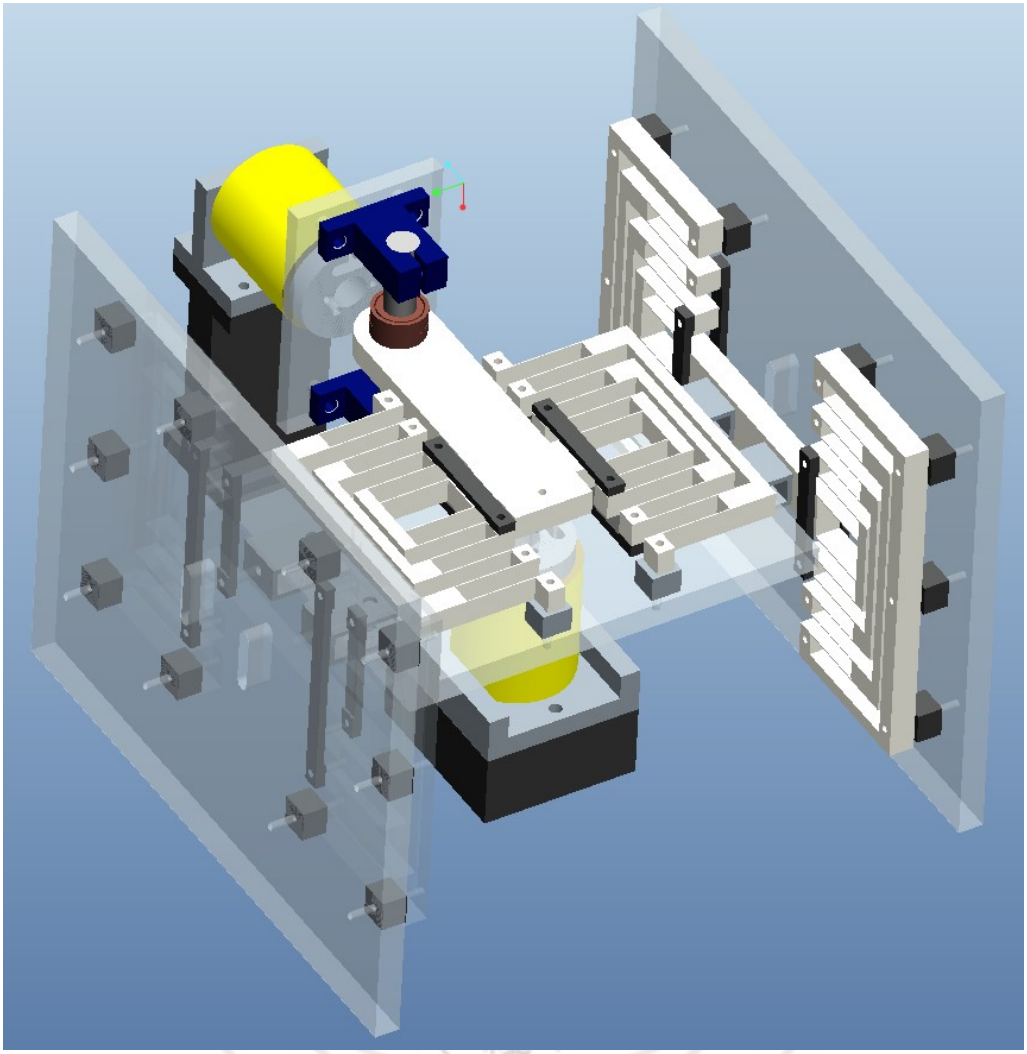

Fig 2. 17 Overview CAD design models of the 2-axis precision alignment machine

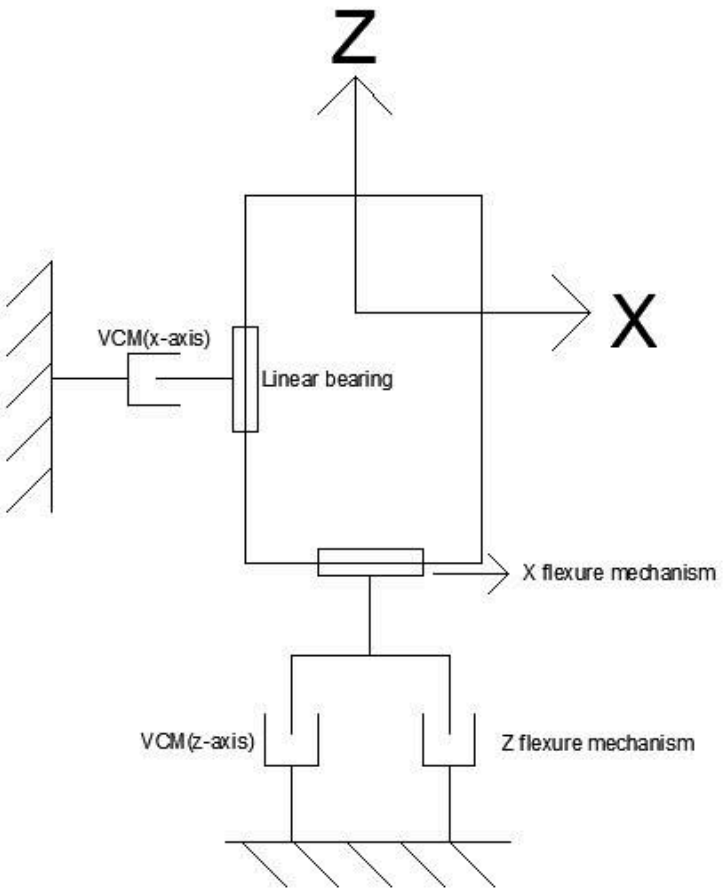

Fig 2. 18 The 2-PP parallel mechanism structure of the machine

CHAPTER 3: SIMULATION STUDY

3.1 THE MATERIAL SELECTION

In the previous chapter, the structures of the machine are determined. For further step, selecting a suitable material is important before the simulation work process. As the designed machine is an elastic-deformation structure and provides the alignment function, so the used material should have high strength and mechanical properties. As the result, the manufacturing material Aluminum 7075-T6 is selected, which is able to meet the aforementioned requirement.

The 7075 aluminum is an aluminum alloy composed by aluminum, zinc, magnesium and copper. Due to its high strength, light in weight and good fatigue strength, the 7075 series aluminum is often used in marine and transport application, even in automotive. The properties of 7075-T6 are shown in Table 3.1. [17]

Table 3. 1 The property of the Al 7075-T6.

Aluminum 7075-T6	
Density	2.81 g/cc
Tensile Yield Strength	503 MPa
Modulus of Elasticity	71.7 GPa
Poisson's Ratio	0.33

3.2 STATIC STRUCTURAL ANALYSIS

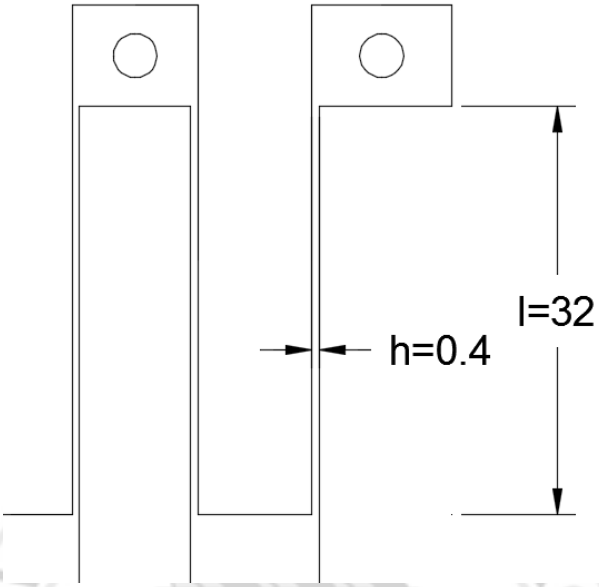

Fig 3. 1The thickness (h) and the length (l) of the leaf-structure (Example for h=0.4mm and l=32mm)

In the previous chapter, the design goal of the required precision range should be ±5mm. Therefore, two conditions are required to be achieved:

(1) The VCM should be able to generate the required driving force to achieve the desired displacement.
(2) The VCM should not break the precision machine during the alignment process.

Referring to the conditions above, a series of finite element model simulations are necessary. By applying the simulation software ANSYS, we can process the designed CAD models, make a completely simulation and data analysis in a designed condition. Thus, according to Fig 3.1, the most desirable value of the thickness (h), and the length (l) of the leaf-structure should be determined using the simulation. As a result, each of

the two axial structures has three different CAD models, which are generated with a fixed length l=28mm and three different of thickness [h=0.4mm, 0.5mm, 0.6mm]. For the simulation, a constant force is required to apply at each model, aiming to prove and determine the best design in those models with different thickness via the simulated result. Also, a 5mm displacement simulation is required to prove that the structure is able to sustain the movement which will not break the material.

In the ANSYS, six models in different thickness have been inserted and a fixed force of 1N and 5mm displacement are applied individually, as shown in Fig.3.2 and Fig. 3.3.

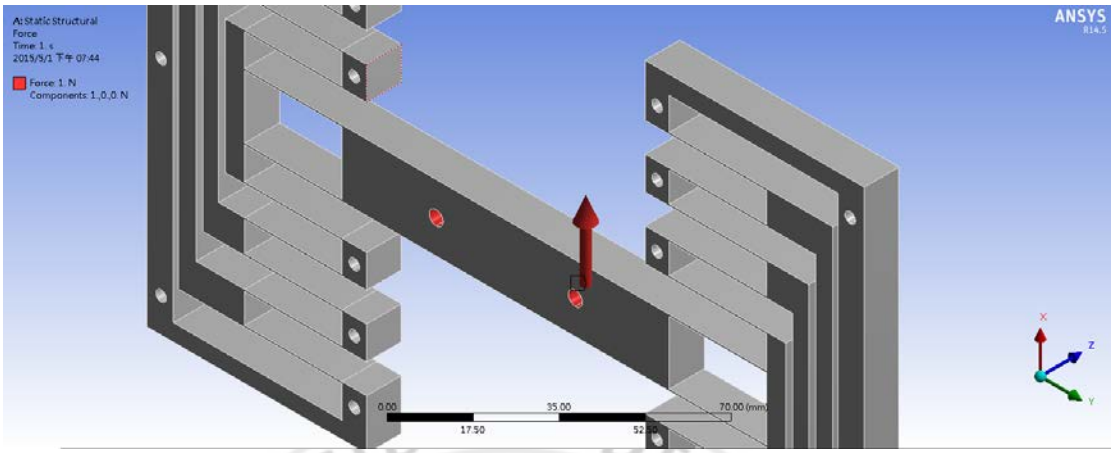

Fig 3. 2 Simulation with a fixed force of 1N acting on the Z-structure.

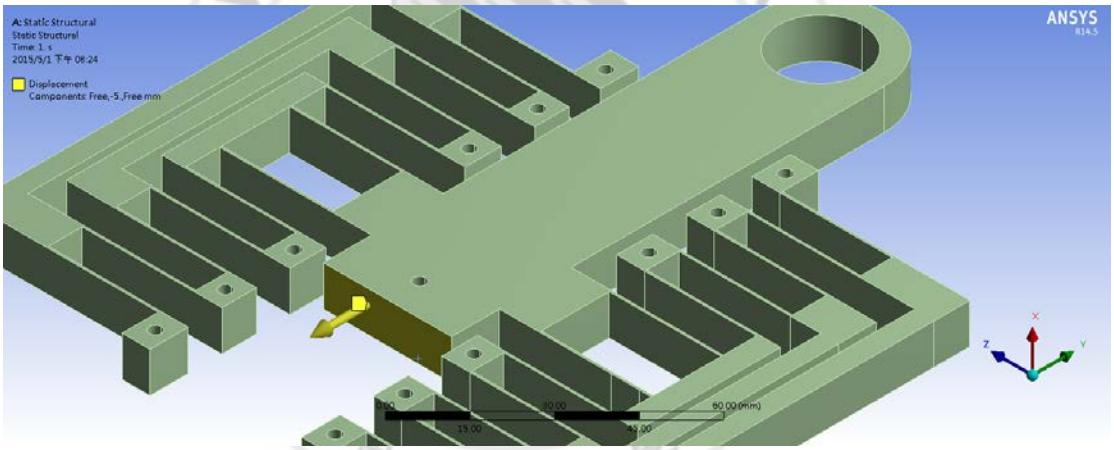

Fig 3. 3 Simulation with a 5mm displacement for the X-structure.

By selecting the material AL7075 and running the simulation, the results of the deformation animation, related maximum equivalent strain and stress are obtained as shown in Fig. 3.4, Fig 3.5 and Fig 3.6, And the results are listed in the Table 3.2 and Table 3.3.

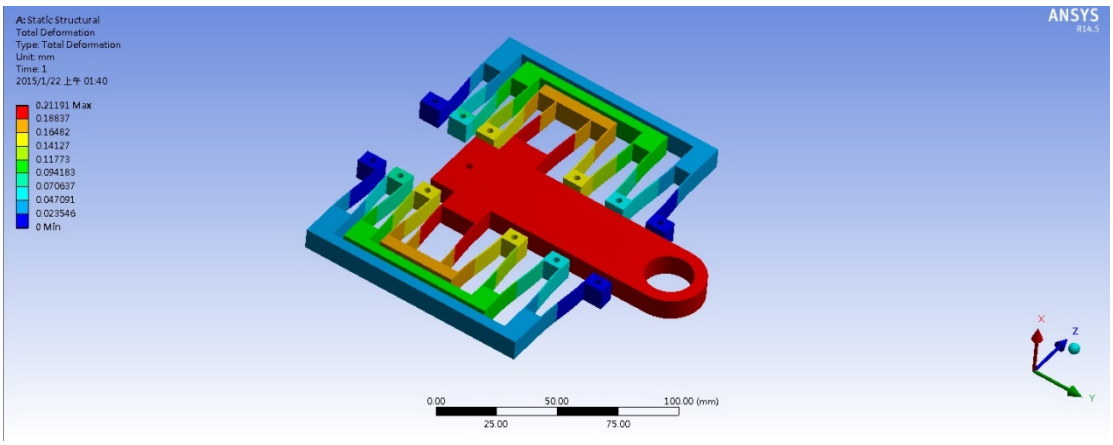

Fig 3. 4 The deformation for 1 N force simulation result in X-structure

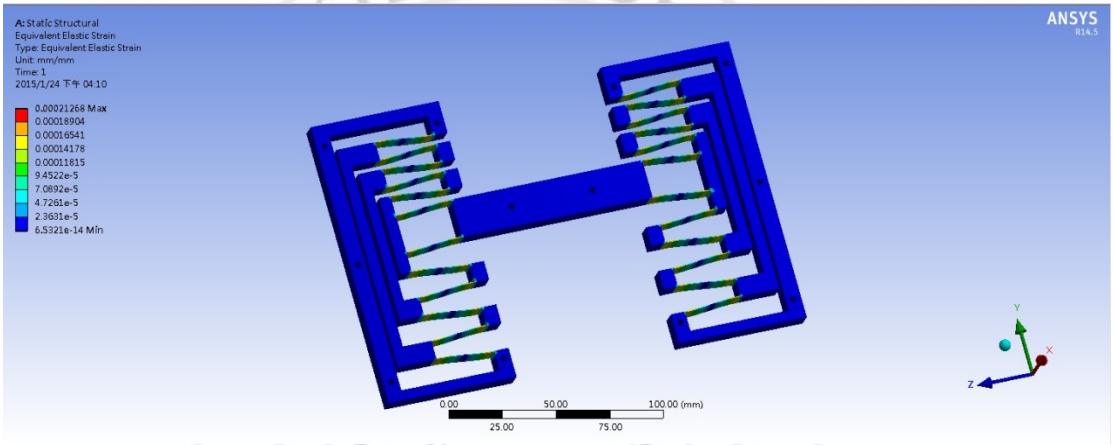

Fig 3. 5 The equivalent elastic strain simulation result in Z-structure

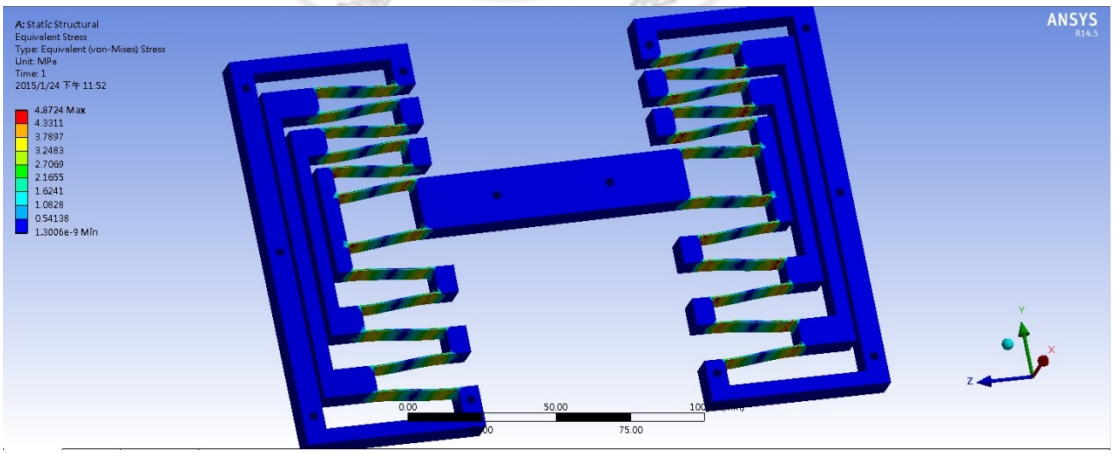

Fig 3. 6 The equivalent stress simulation result in Z-structure

Table 3. 2 X-axis structure Ansys result with a constant force of 1 Newton

	0.6mm thickness	0.5mm thickness	0.4mm thickness
Displacement (mm/N)	0.21191	0.36034	0.69482
Elastic Strain (mm/mm)	9.2944×10^{-5}	1.2449×10^{-4}	2.1638×10^{-4}
Stress (MPa)	6.6534	8.9072	15.492

Table 3. 3 Z-axis structure Ansys result with a constant force of 1 Newton.

	0.6mm thickness	0.5mm thickness	0.4mm thickness
Displacement (mm/N)	0.19137	0.30148	0.69528
Elastic Strain (mm/mm)	6.8111×10^{-5}	1.0305×10^{-4}	2.1268×10^{-4}
Stress (MPa)	4.8724	7.3085	15.224

For the results above, the displacement in different thickness structure by 1 newton has been obtained. As the result, the force is required to generate by the VCM is calculated by:

*Force required to generated = Displacement estimate * Newton per Displacement*

The safety factor is calculated by:

Safety factor = Yield Strength / Current maximum stress

Table 3. 4 The safety factor, force required, maximum stress result for X-axis structure

	0.6mm thickness	0.5mm thickness	0.4mm thickness
Newton per Displacement(N/mm)	4.719	2.775	1.439
Force required (N)	23.595	13.876	7.196
Max. Stress (MPa)	156.94	123.86	111.51
Safety factor	3.205	4.061	4.511

Table 3. 5 The safety factor, force required, maximum stress result for Z-axis structure

	0.6mm thickness	0.5mm thickness	0.4mm thickness
Newton per Displacement(N/mm)	5.225	3.317	1.438
Force required (N)	26.1274	16.58485	7.191347
Max. Stress (MPa)	136	121.69	109.44
Safety factor	3.699	4.133	4.596

Table 3. 6 The details for the VCM NCC05-18-060-2X

MOVING COIL NON-COMM ACTUATOR SPECIFICATIONS		
Motor P/N	NCC05-18-060-2X	
Stroke	0.50"	12.7 mm
Radial Clearance	0.015" per side	0.38 mm per side
Bearing Type	None Provided	
Moving Mass	0.22 lbs	99 grams
Total Mass	1.20 lbs	544 grams
Resistance @ 20C	11.5 ohms	
Inductance @ 20C	4.5 mH	
Electrical Time Constant	0.39 msec	
Motor Constant	1.78 LBS/SQRT(Watt)	7.92 N/SQRT(Watt)
Force Constant	6.3 LBS/Amp	27.8 N/Amp
Back EMF	0.7 V/ips	27.8 V/m/sec
Continuous Force	6.0 LBS	26.7 N
Max Power @ 100% Duty	12 Watts	
Peak Force	18.0 LBS	80.1 N
Max Power @ 10% Duty	102 Watts	

The displacement, required force, the safety factor and the maximum stress of the structures are obtained and listed in Table 3.4 and 3.5. From the specification of the VCM, the peak force is 80.1 N, so it can provide adequately driving force to reach the ±5mm displacement. Also, the equivalent stress for all CAD models is lower than the Al-7075 break point, so the machine would not be damaged and broken during the alignment procedure.

3.3 THE CONCLUSION AFTER THE SIMULATION

From the previous simulation results, the simulation sufficiently expresses the performance of the designed models and proves that the applied material is suitable for the prototype. Overall, all the models can provide well performances and lead to achieve the goal, especially the 0.4mm thickness model can provide a higher safety factor and require less force to obtain the goal. However, due to the machining company's limitation of technique, 0.5mm thickness is the minimum selection. As the result of it, the length in 26mm and thickness in 0.5mm is the final decision of the design.

CHAPTER 4: THE PROTOTYPE ASSEMBLY

Since the simulation study and the determination of the model parameters are done in the previous chapter, a prototype should be manufactured and assembled based on the result. The three main leaf-structures (one X-axis structure and two Z-axis structures), the acrylic sheet basements and the other parts are manufactured by several machining companies in mainland China. Finally, the assembly work of the prototype was done after the parts are well received, as shown in Fig. 4.1, 4.2 and 4.3. It is accorded with the CAD model assembly design. Appendix A describes the used hardware components in detail.

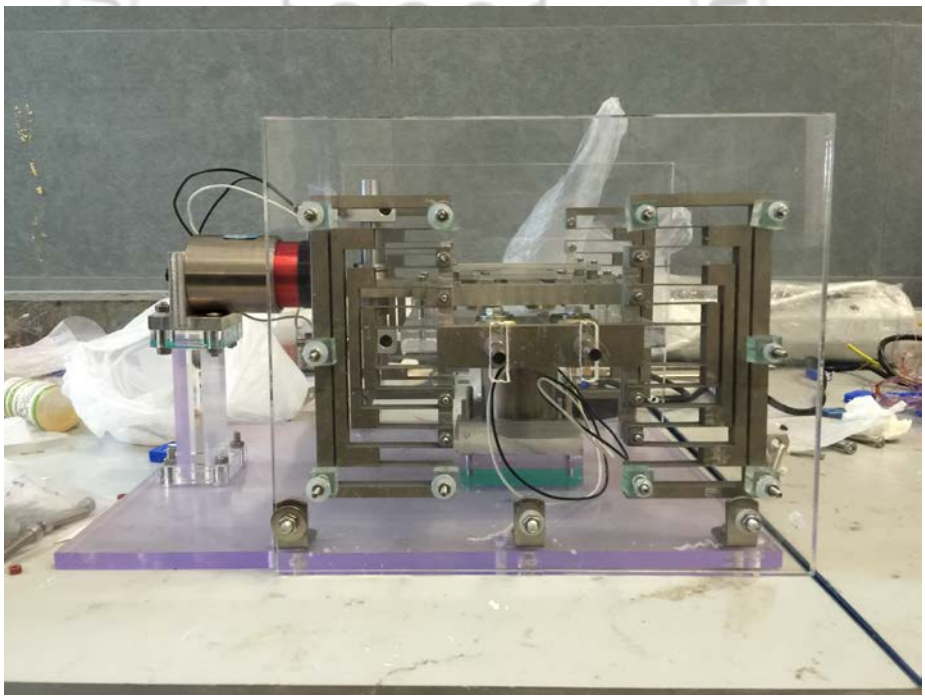

Fig 4. 1 The front view of the prototype.

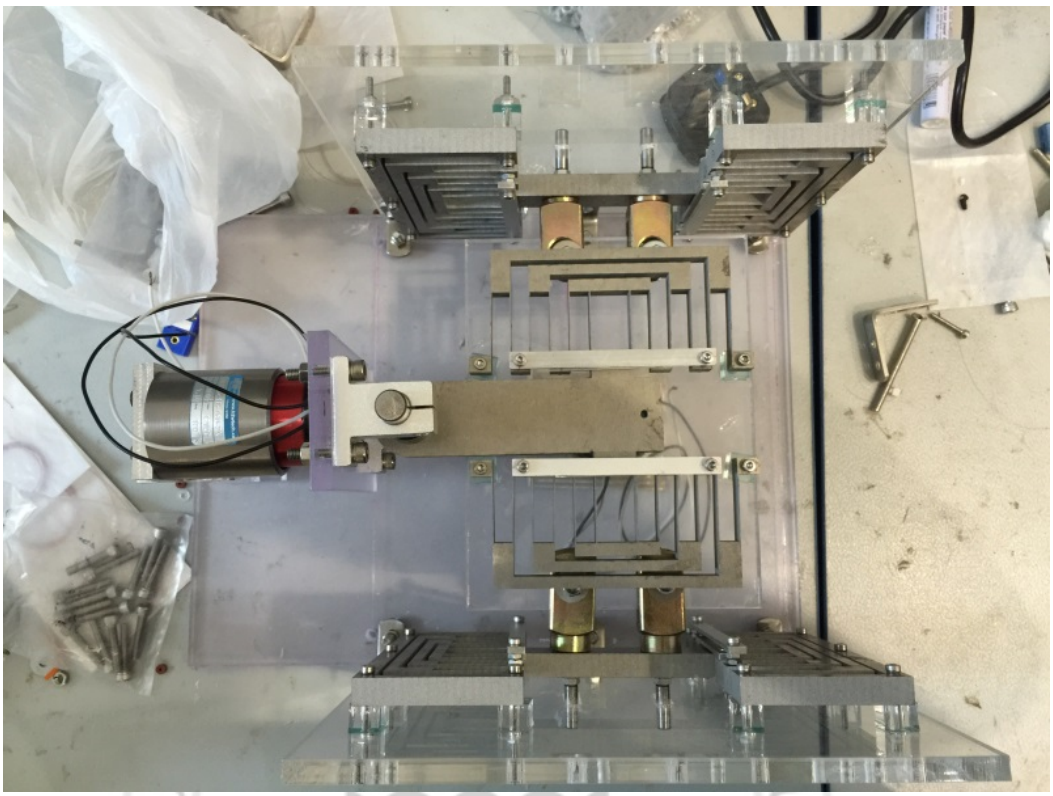

Fig 4. 2 The top view of the prototype

Fig 4. 3 The side view of the prototype.

CHAPTER 5: EXPERIMENT STUDY OF THE TWO-AXIS PRECISION ALIGNMENT MACHINE

5.1 EXPERIMENT OF DISPLACEMENT AND DECOUPLING

A block diagram of the experimental setup is shown in Fig 5.1. The goal of the experiment study is to verify whether the prototype is able to achieve the aforementioned goal. Moreover, a camera is installed to simulate the application of the precision function for the image focusing. The combined experimental setup is shown in Fig. 5.2.The measurement of the displacement relies on two laser sensors and its monitor driver. The LabVIEW software running in a PC will generate a voltage to be applied to the VCM driver and receive the signal from the sensor conditioner via the RS232 connection simultaneously. Thus, the VCM will provide a linear driving motion based on the particular voltage. As the result of it, the relationship between the voltage and the displacement will be easily obtained.

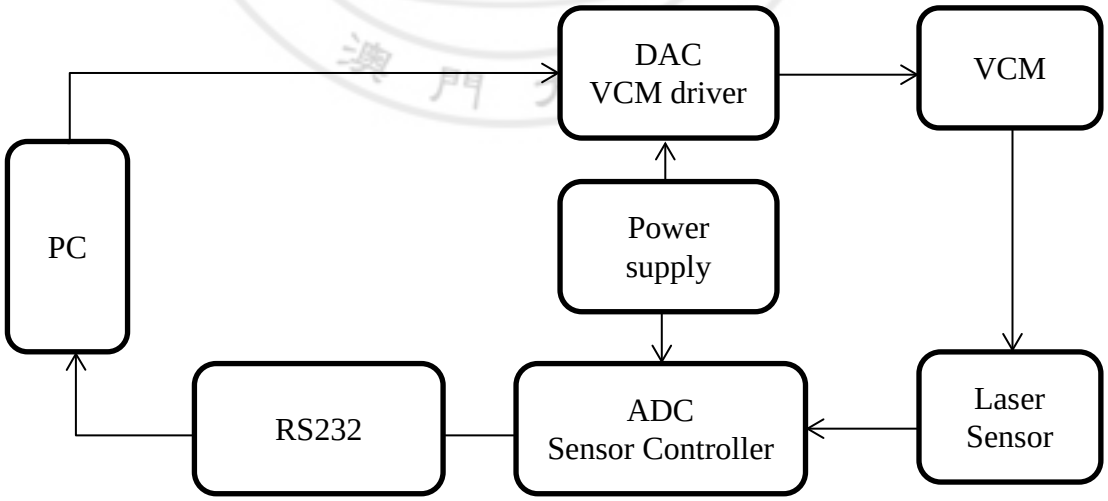

Fig 5. 1 The block diagram of the experimental setup flow chart

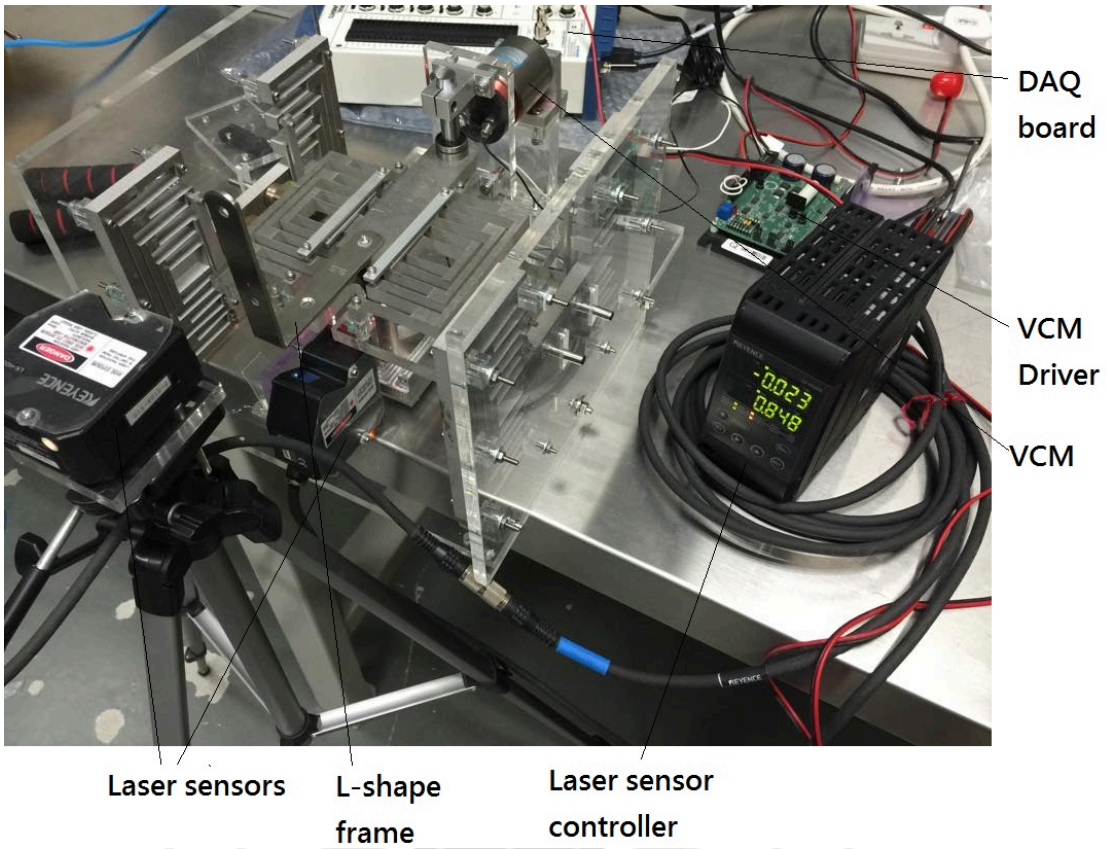

Fig 5. 2 The combined experimental setup of all equipment

Firstly, an individual displacement experiment for each axial-structure is required, which provides a continuous voltage to the VCM and drives the structure moving. Then, the laser sensor detects the variation in displacement and records it. A sine wave voltage in amplitude of 5V is generated for both X and Z axial structures. It is found that the moving range of each structure is about 12mm (shown in Fig. 5.3 and 5.4). That means that the design has achieved the goal for over 10mm precision range.

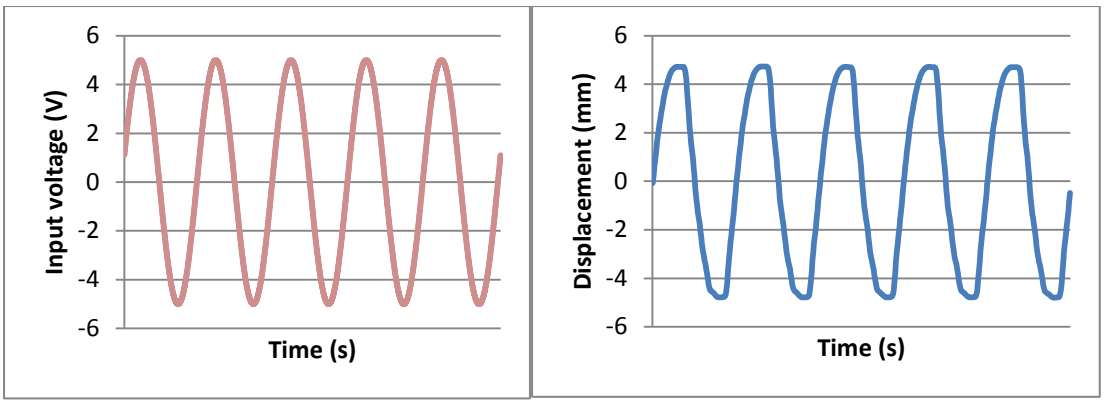

Fig 5. 3 The experimental result for the X-axis structure

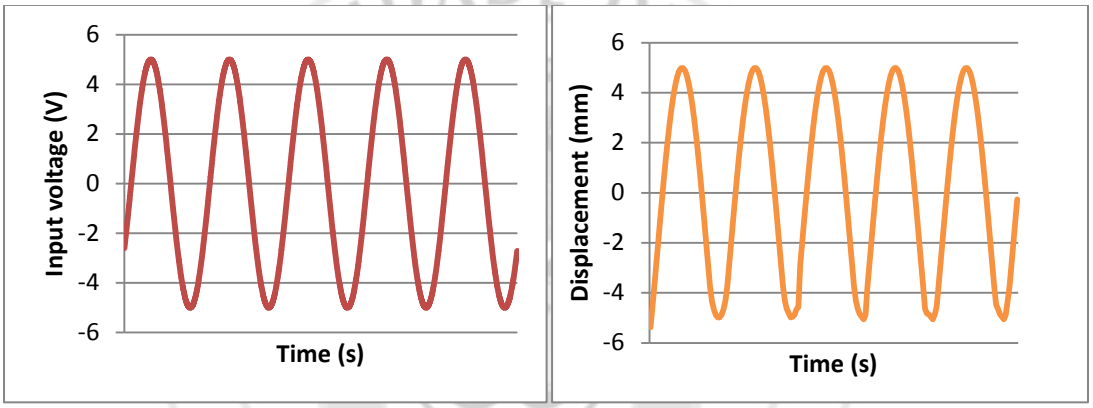

Fig 5. 4 The experimental result for the Z-axis structure

For the next step, it is to determine whether the prototype is successful decoupled and is able to provide a two-axial precision alignment function or not. One of the VCM will drive the structure in sine curve voltage and the two laser sensors will record both two structures displacement simultaneously. As the goal mentioned in the previous chapter, the total displacement of the minor axis structure should not larger than 1 % to the major one or it fails. The error percentage can be calculated:

$$\text{Error percentage} = \frac{\sum_1^n |minor\ axis\ displacement|}{\sum_1^n |major\ axis\ displacement|} \times 100\%$$

After the experiment, the result are recorded and shown in Fig 5.5 and 5.6. Also the error percentage of X and Z axial structures are calculated, shown in Table 5.1. The result showed that both X and Z axial structures have error percentage about 0.2%, which is far below to the minimum requirement 1%. That means that the prototype is well-decoupled and is able to give two-axis precision work.

Table 5. 1 The result of error percentage

	Error percentage (%)
X-Z experiment (X-axis is major)	0.1947
Z-X experiment (Z-axis is major)	0.2048

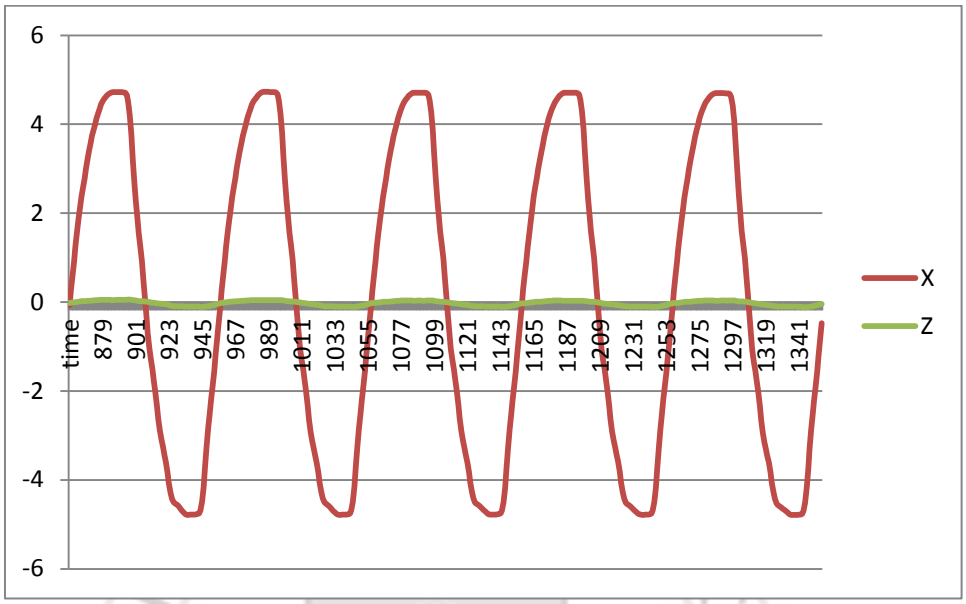

Fig 5. 5 The result with X-Z axial displacement where X is the major driving unit

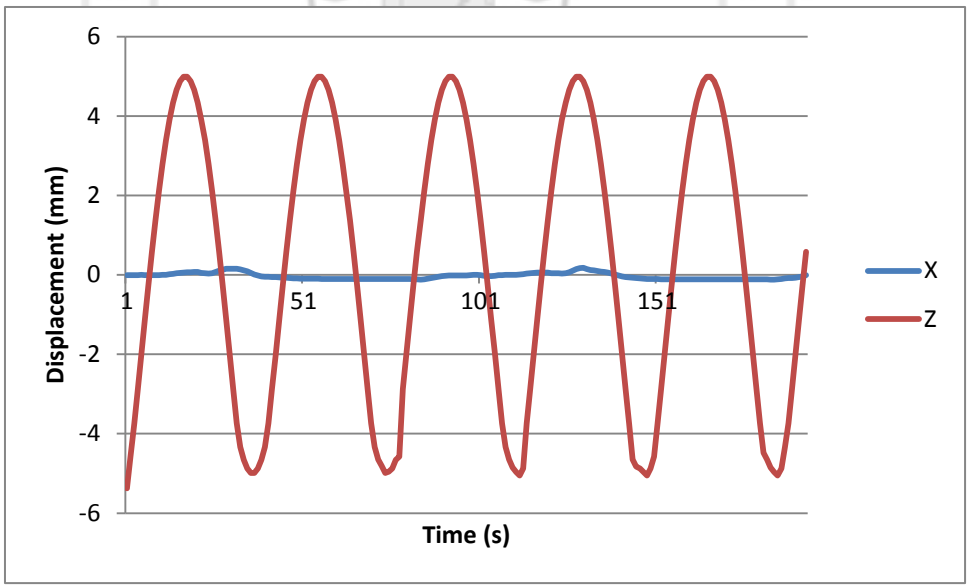

Fig 5. 6 The result with Z-X axial displacement where Z axis is the major driving unit

5.2 Application Experiment in Image Focusing

In order to simulate and approve that the function of the prototype, an image focusing experiment is set up. A camera is installed on the X-leaf structure and placed before a paper with some ‘X’ (shown in Fig 5.7), the camera is out of focus and the images recorded are indistinct. By applying the experiment in the previous experiment, the image has successfully be more distinct once the X-leaf structure moves forward (shown in Fig 5.8). The experimental results verify the application of the machine.

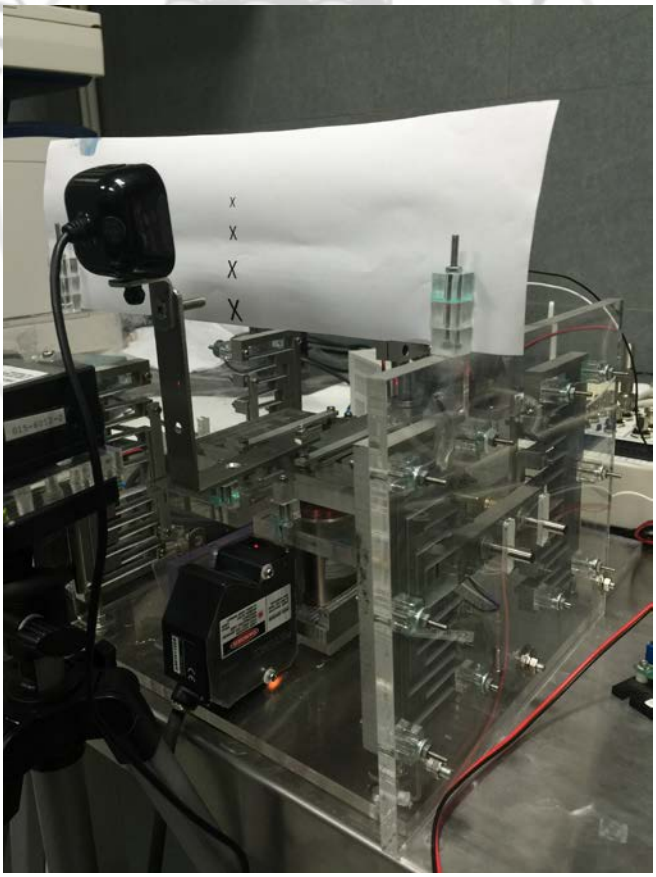

Fig 5. 7 The experimental setup for the camera and the paper.

Fig 5. 8 The comparison for the image focusing experiment.

CHAPTER 6: CONCLUSION

The project presents the design and development procedures of a two-axis micro-motion machine for precision alignment. By analyzing and determining the mechanism design, the material selection, simulation study and experimental testing are carried out. Results show that the design satisfies the goal and requirement. Due to the hardware constraint, the prototype dimension is 250mm x 350mm. It provides a precision range over 10mm and is well-decoupled, which achieves general application requirement condition. The prototype is assembled for the experimental study. In the experiment, the relationship between the voltage input and the displacement of the structure is distinctively reached. In addition, the image focusing experiment indicates that the prototype is able to provide the focus function to something that is out of focus. Finally, the error percentage has been calculated by 0.2%. This error is majorly caused by artificial assembly and the latent problem, which may influence the fitness between the parts.

The main contribution and the advantage of the design is that the prototype can provide a movable, non-friction, light in net weight and stable precision alignment stage for an object to give the adjustment function. Moreover, the design has extended the multi-stage parallel micro-positioning system and augmented with a serial of mechanism structure, which gives a useful reference to the alignment instrument design in future.

REFERENCES

[1] M. Gauthier and E. Piat, “Control of a particular micro-macro positioning system applied to cell micromanipulation,” *IEEE Trans. Automat. Sci. Eng.*, vol. 3, no. 3, pp. 264-271, 2006.

[2]W. O’Brien, “Long-range motion with nanometer precision,” *Photonics Spectra*, Laurin Publishing Co. Inc., pp. 80-81, 2005.

[3] G. Dai, F. Pohlenz, H.-U. Danzebrink, M. Xu, K. Hasche, and G. Wilkening, “Metrological large range scanning probe microscope,” *Review of Scientific Instruments*, vol. 75, no. 4, pp. 962-969, 2004.

[4] J. A. Kramar, “Nanometre resolution metrology with the molecular measuring machine,” *Measurement Science & Technology*, vol. 16, no. 11, pp. 2121-28, 2005.

[5] K. Salaita, Y. H. Wang, and C. A. Mirkin, “Applications of dip-pen nanolithography,”*Nature Nanotechnology*, vol. 2, no. 3, pp. 145-55, 2007.

[6] T. Hausotte, G. Jaeger, E. Manske, N. Hofmann, and N. Dorozhovets, “Application ofa positioning and measuring machine for metrological long-range scanning force microscopy,” *Proc. of SPIE*, vol. 5878, p. 587802, 2005.

[7] A. Sinno, P. Ruaux, L. Chassagne, S. Topcu, and Y. Alayli, “Enlarged atomic force microscopy scanning scope: novel sample-holder device with millimeter range,” *Review of Scientific Instruments*, vol. 78, no. 9, pp. 09517, 2007.

[8] A. Weckenmann and J. Hoffmann, “Long fange 3D scanning tunneling microscopy,” *CIRP Annals - Manufacturing Technology*, vol. 56, no. 1, pp. 525-528, 2007.

[9] Q.Xu, “Design and development of a compact, flexure-based *XY* precision positioning system with centimeter range,” *IEEE Trans. Ind.Electron.* vol. 61, no. 2, 2014.

[10] C. Kim, M.-G. Song, Y.J. Kim, N.-C. Park, K.-S. Park, Y.-P. Park, K. S. Shin, J. G. Kim, and G. S. Lee, “Design of an auto-focusing actuator with a flexure-based 45 compliant mechanism for mobile imaging devices,” *Microsyst. Technol.*, vol. 19, pp. 1633-1644, 2013.

[11] nPoint, 2004, "*Nanopositioning Tools and Techniques for R&D Applications*," nPoint, Inc., Madison, Wisconsin.

[12] A.-C. Zhang, X.-H. Xie, and Y.-L. Wu, “Design of double-axis halfellipse flexure hinge,” *Aviation Precision Manufacturing Technology*, vol. 42, no. 5, pp. 15-18, 2006.

[13] J. K. Jung, W. S. Youm, K. H. Park, “Vibration reduction control of a voice coil motor (VCM) nano scanner,*” Int. J. Precision Engineering and Manufacturing*, vol. 10, no. 3, pp. 167-170. 2009.

[14] C. S. Liu, P. D. Lin, “Miniaturized auto-focusing VCM actuator with zero holding current”, *Optics Express*, vol. 17, no. 12, pp. 9754-9763, 2009.

[15] http://218.58.156.215:1003/jiaoan/16.htm

[16] Slocum, A. H., 1992, *Precision Machine Design*, Society of Manufacturing Engineers, Dearborn, MI.

[17] http://www.matweb.com/search/DataSheet.aspx?MatGUID=9852e9cdc3d4466ea9f111f3f0025c7d&ckck=1

[18] Yilin Liu, Kailin Wu, Da Xu, and Qingsong Xu, “Design of a Microscope Auto-Focusing Device Based on Multi-Stage Leaf Spring”, *IEEE International Conference on Information and Automation (ICIA 2014)*, July 26-31, 2014, Inner Mongolia,Chin.

[19] Dr. Q. Xu, “New flexure parallel-kinematic micropositioning system with large workspace,” *IEEE Trans. Robotics*, vol. 28, no. 2, pp. 478-491, 2012.

[20] Y. Li, Q.Xu, ”Design and Robust Repetitive Control of a NewParallel-Kinematic XY Piezostage forMicro/Nanomanipulation,” *IEEE Trans.Mechatronics*, pp 1-13, 2011.

APPENDIX A: THE HARDWARE COMPONENTS IN CAD DRAWING

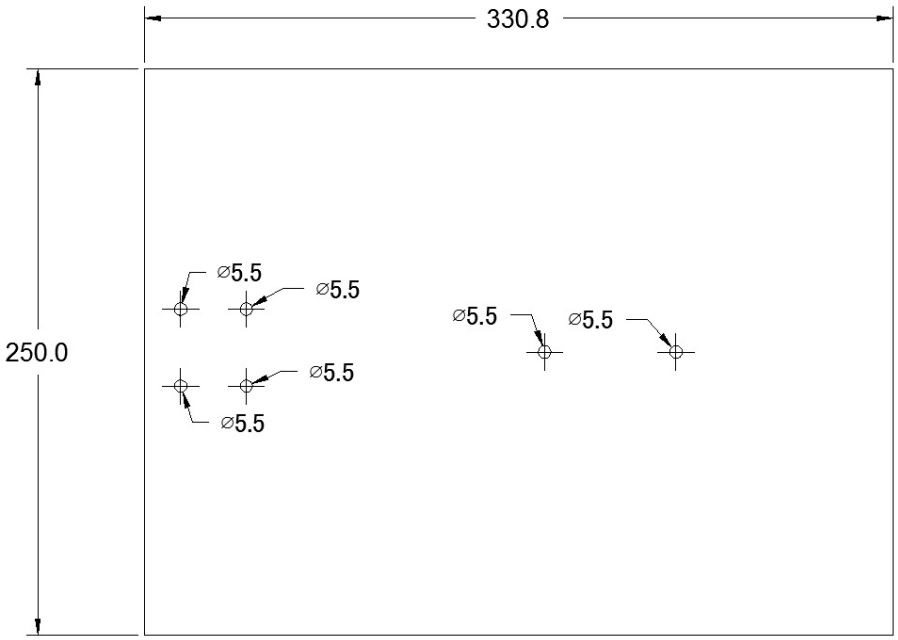

Fig A. 1 The base

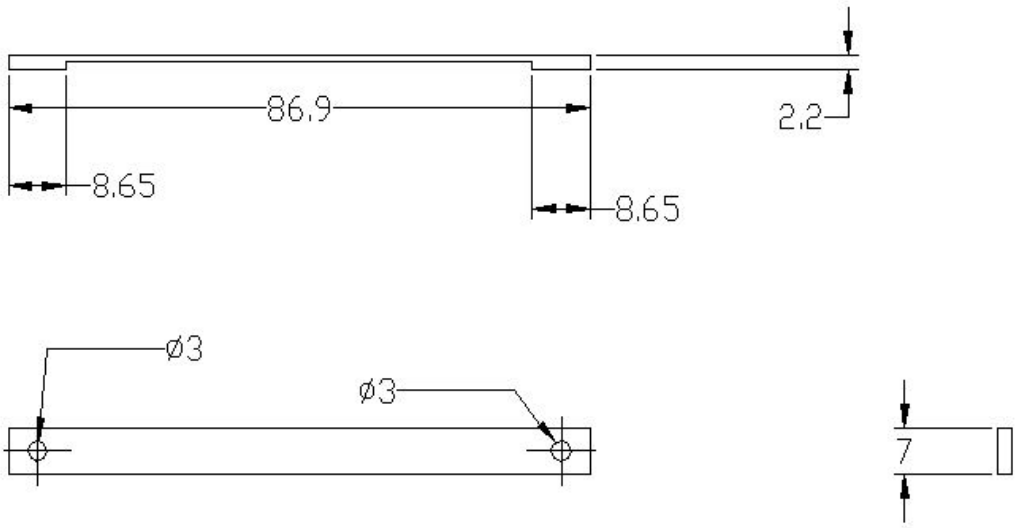

Fig A. 2 The short bridge of X-axis.

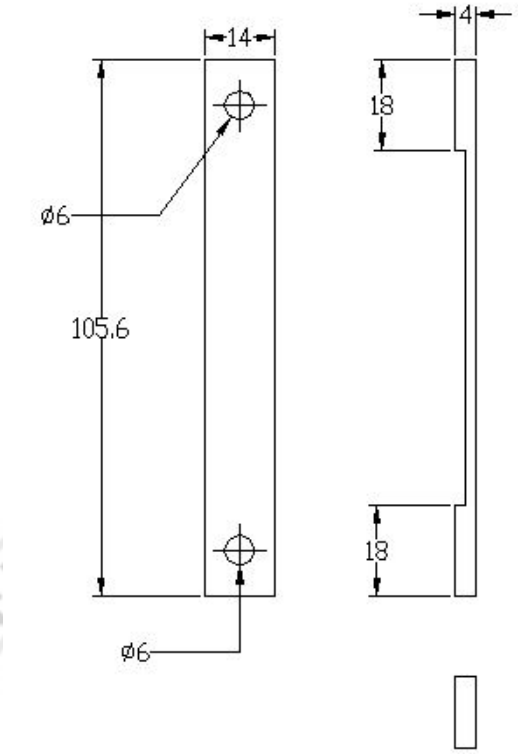

Fig A. 3 The long bridge of X-axis.

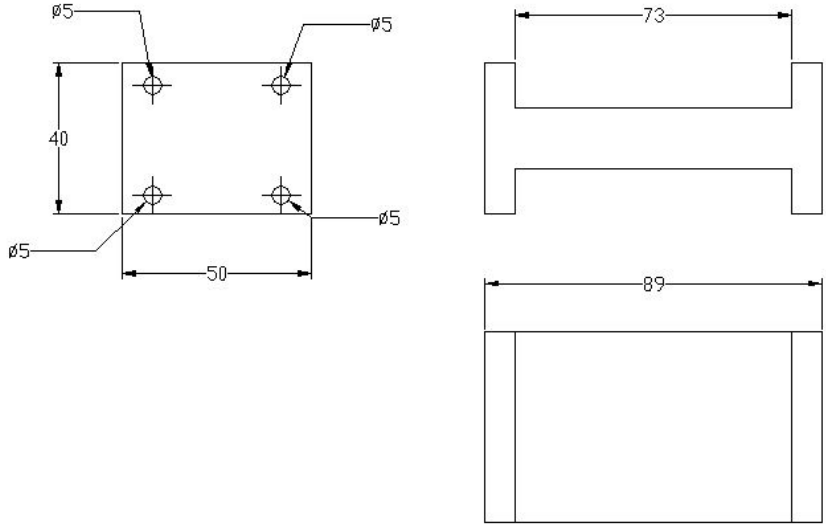

Fig A. 4 The X-coil down support

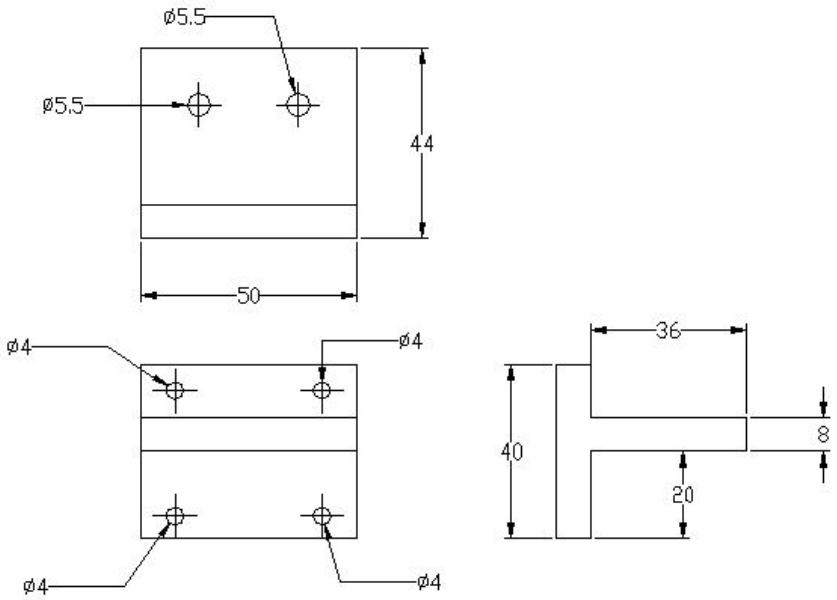

Fig A. 5 The X-coil support

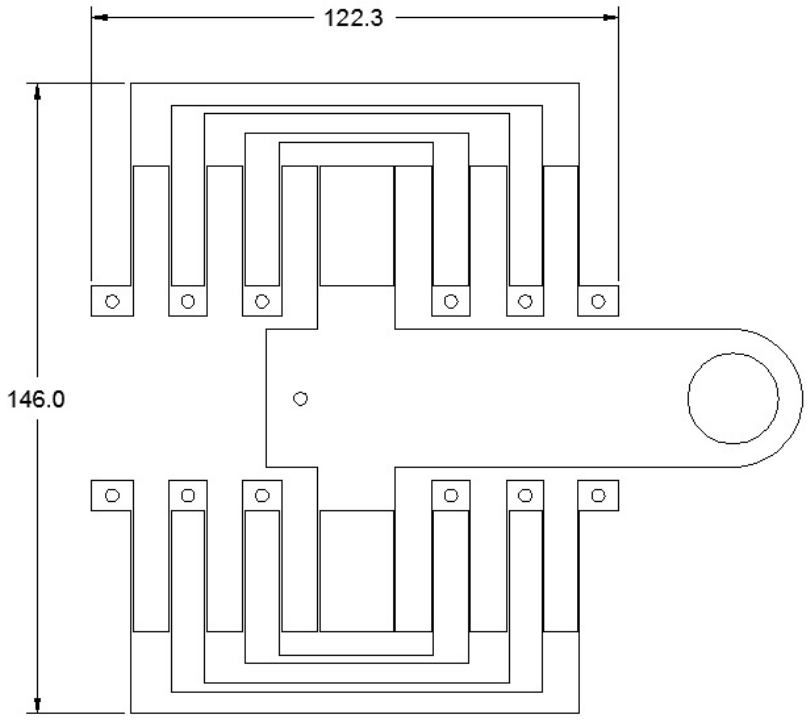

Fig A. 6 The X-platform

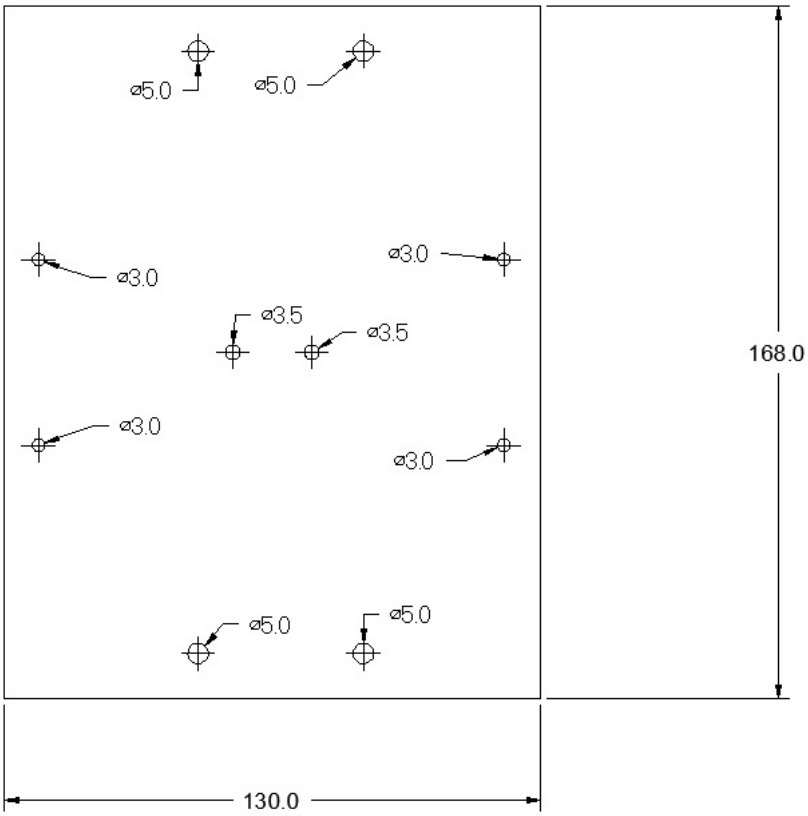

Fig A. 7 The X-platform holder

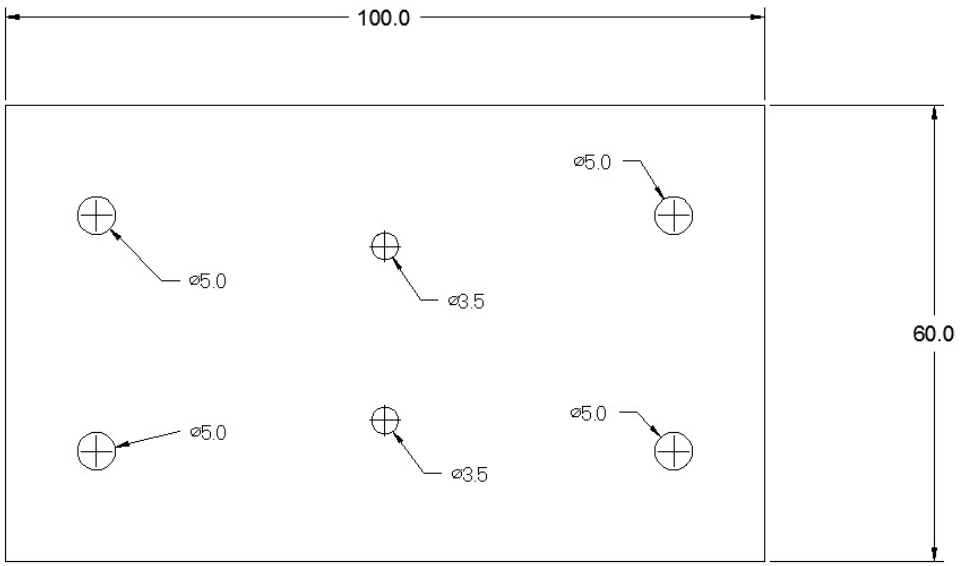

Fig A. 8 The Acrylic Sheet which push the X-platform

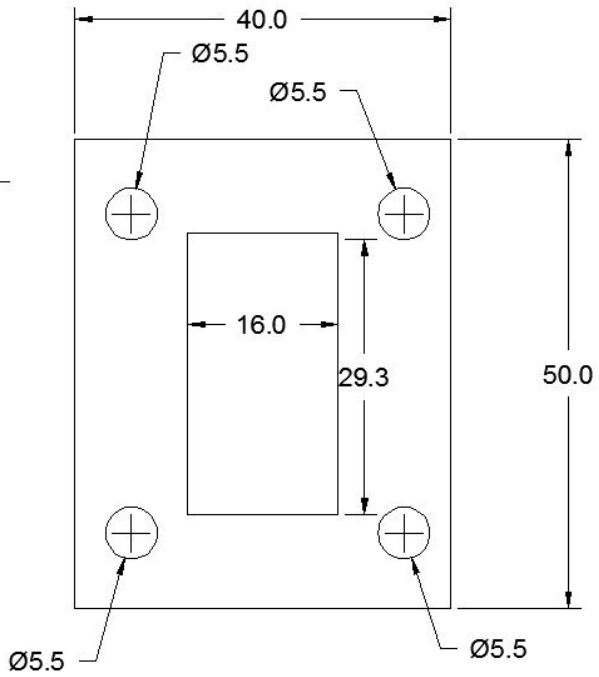

Fig A. 9 The bottom of the X-support 1

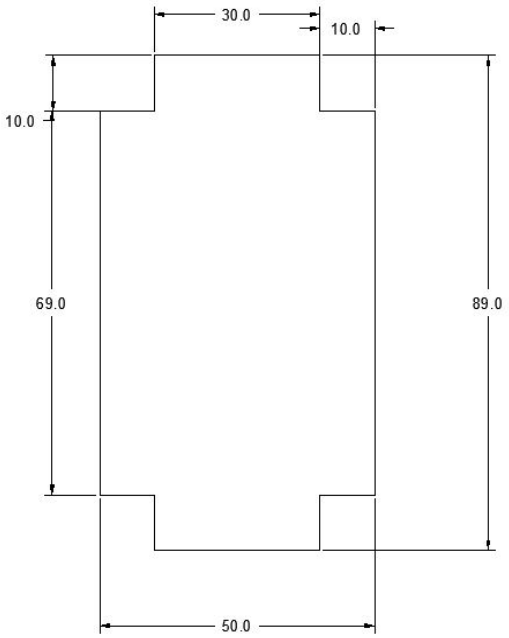

Fig A. 10 The bottom of the X-support 2

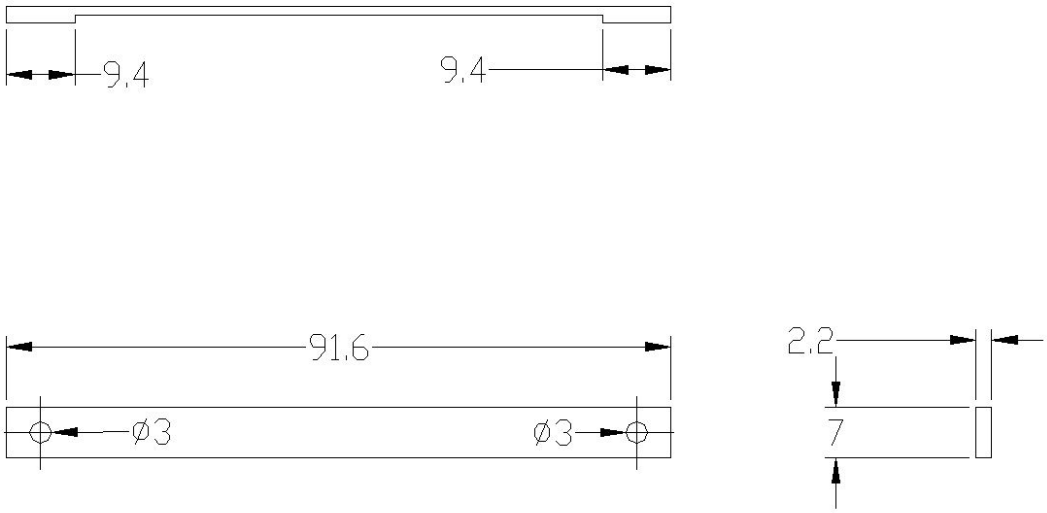

Fig A. 11 The short bridge of Z-axis.

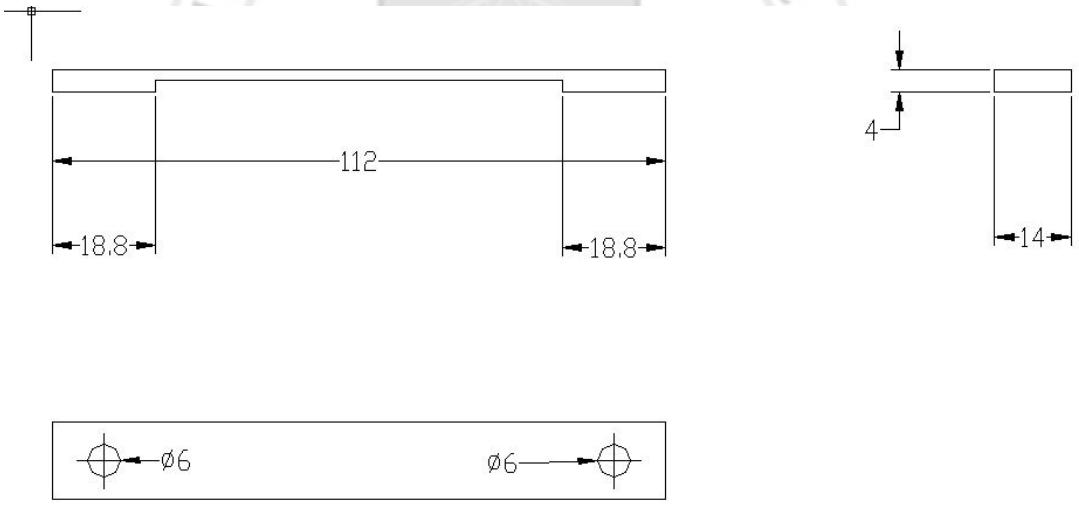

Fig A. 12 The long bridge of Z-axis.

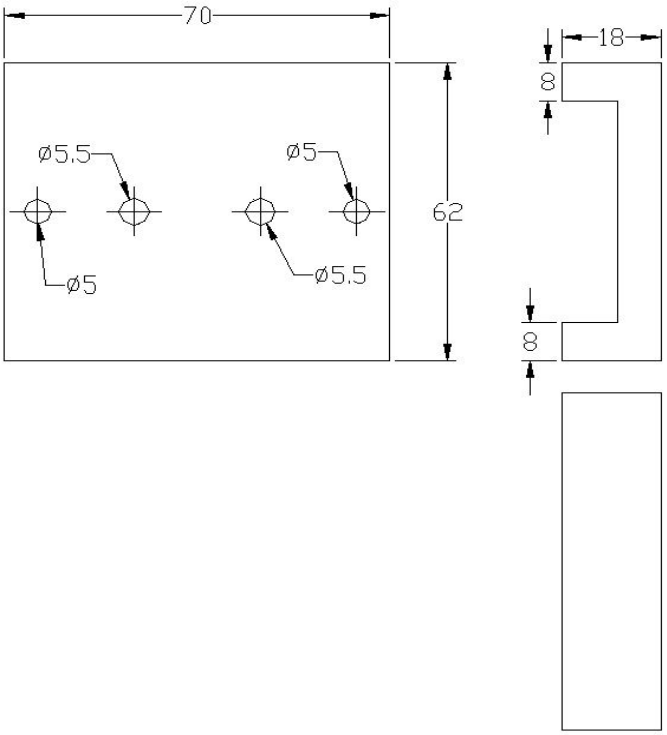

Fig A. 13 The Z-coil support

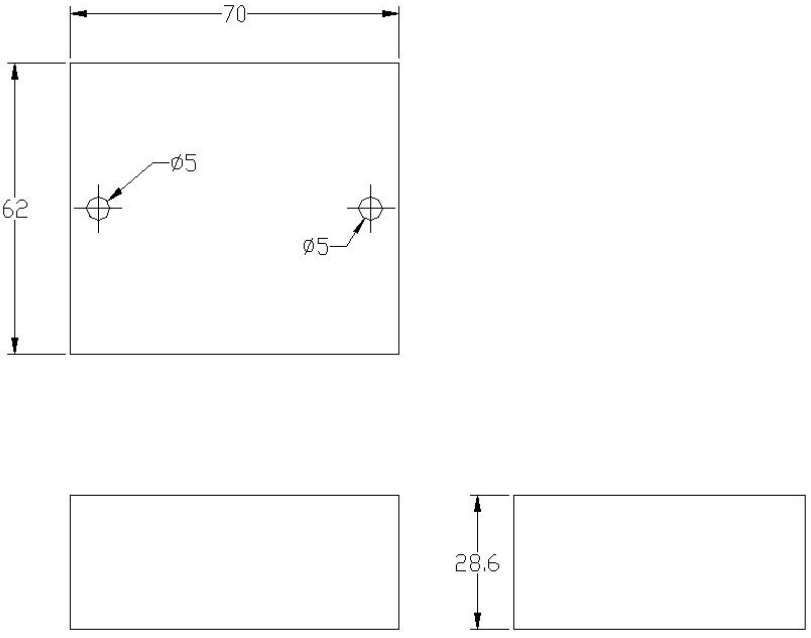

Fig A. 14 The Z-coil down support

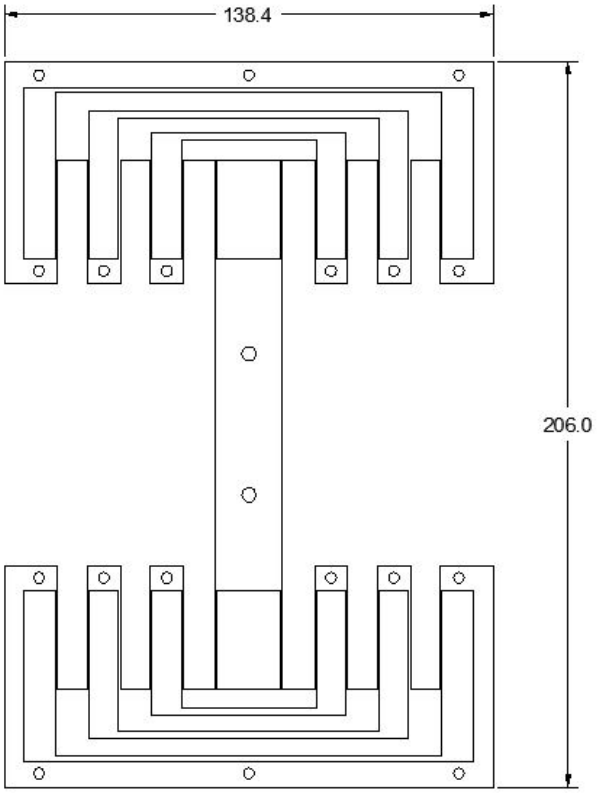

Fig A. 15 The Z-platform

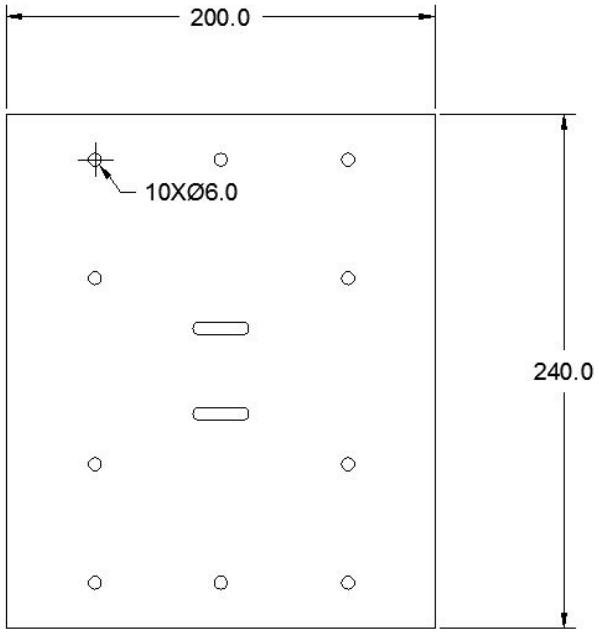

Fig A. 16 The Z-platform holder

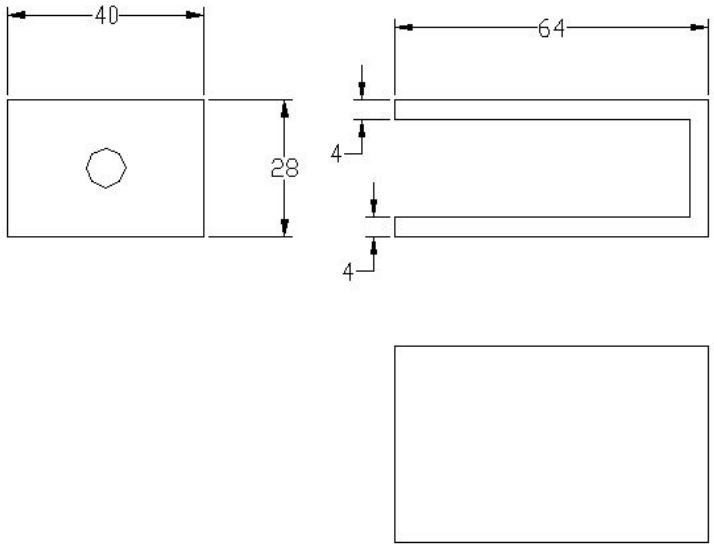

Fig A. 17 The U-shape supports

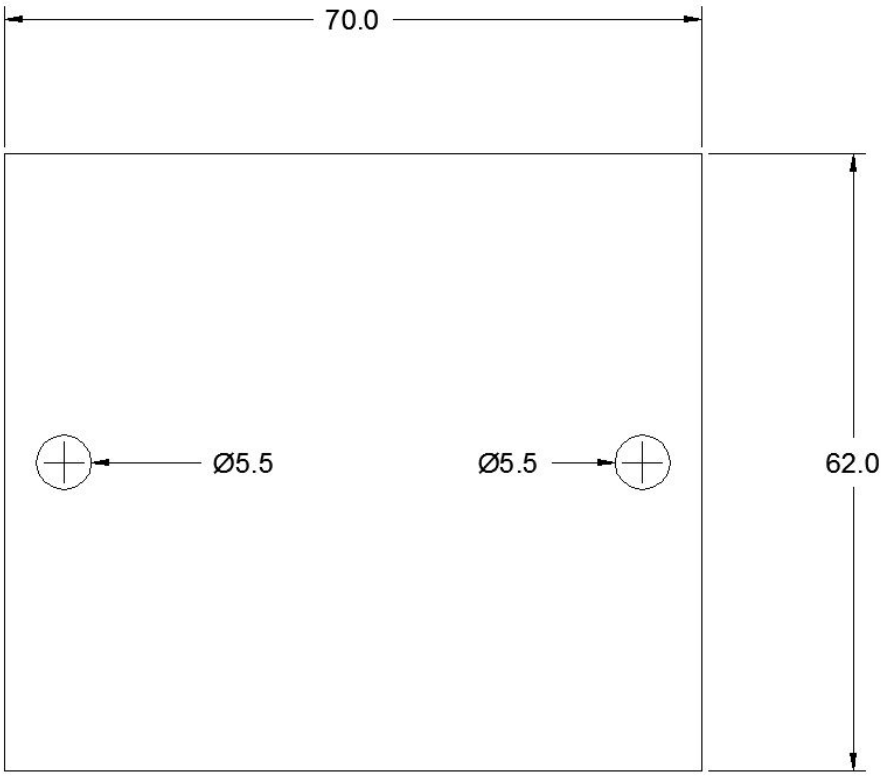

Fig A. 18 The bottom part of Z-support.

APPENDIX B: COMPONENTS OF THE WORKING STAGE

(a)

(b)

(c)

(d)

(e)

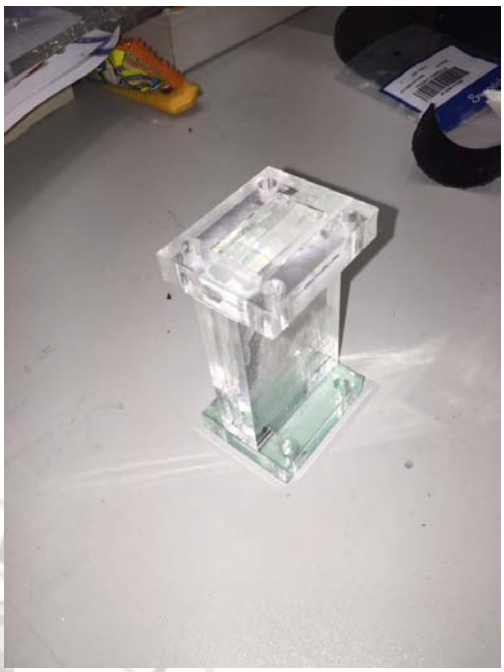

(f)

(g)

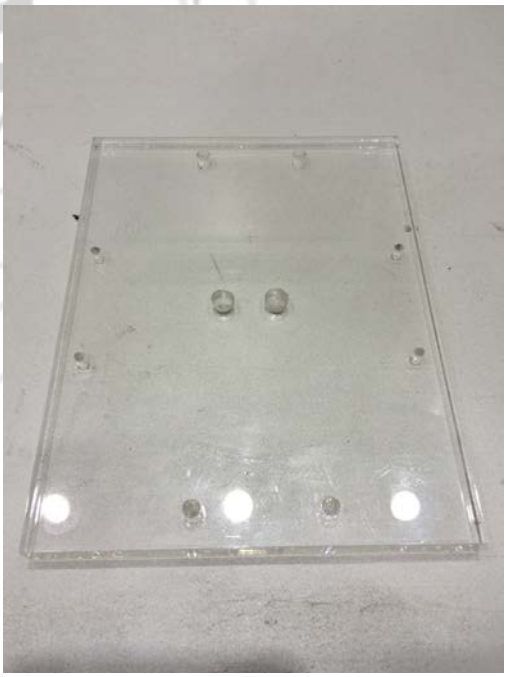

(h)

(i)

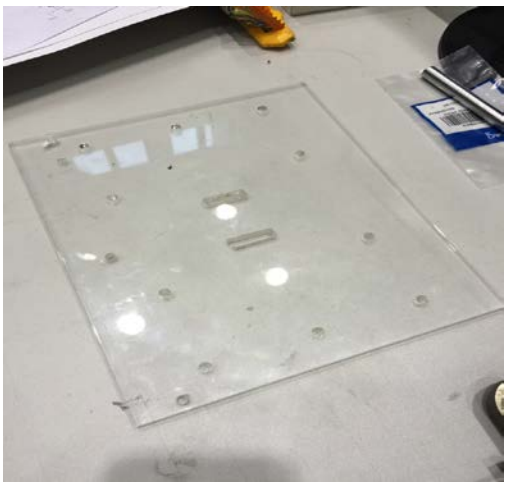

(j)

(k)

(l)

Fig B. 1 (a)Z-Platforms (b)Holders (c) X-Coil Support (d)Z-Coil Support (e)X-Platform (f)X-Coil Down Support (g)Optical Axis (h)The X-Platform Holder (i)Base (j)Z-Platform Holders (k)U-Shape Supporters (l)Long And Short Bridges

APPENDIX C: EXPERIMENT DEVICES LIST

The experiment hardward for collecting date are listed as below:

Laser sensor: LK-H055, Keyence Inc.

VCM: NCC05-18-060-2X, H2W Inc.

Controller: NI CRIO9075, National Instruments Inc.

ADC: NI 9215, National Instruments Inc.

DAC: NI 9263, National Instruments Inc.

Camera: C298 20M pixels HD high Definition Webcam

APPENDIX D: WORK BREAKDOWN

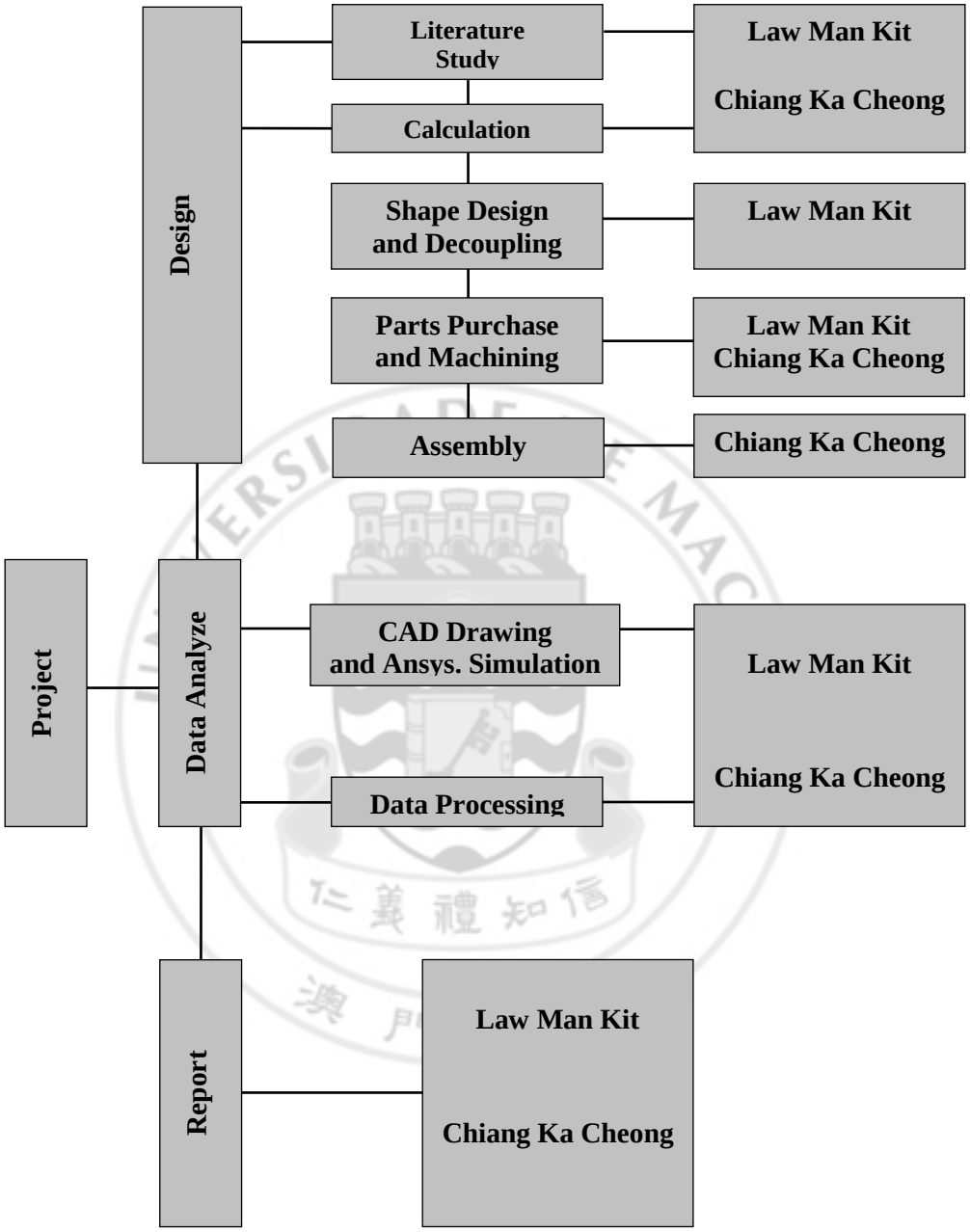

APPENDIX E: PUBLICATION

1. Man Kit Law, Ka Cheong Chiang, and Qingsong Xu, “Design and Fabrication of a Two-Axis Micro-Motion Machine for Precision Alignment”, *IEEE International Conference on Information and Automation (ICIA 2015),* August 8-10, 2015, Yunnan, China (to be Indexed by ISI-CPCI, EI Compendex, IEEE Xplore), submitted.